공학박사학위논문

유도가열을 통한 항공기 구조물 복합재 패치 접착수리

Repair of Aircraft Structures Using Composite Patches Bonded Through Induction Heating

2014 년 2 월

서울대학교 대학원

기계항공공학부

김 민 호

Repair of Aircraft Structures Using Composite Patches Bonded Through Induction Heating

Min Ho Kim
School of Mechanical and Aerospace Engineering
Seoul National University

Abstract

With the increasing aging aircraft, many unanticipated structural defects have been occurred in aircraft. Accordingly, many aircraft structural repair methods have been developed, but we need efficient method except for conventional repair method as mechanical riveting. This paper presents research on composite patch repair to damaged aluminum aircraft structure. Composite patches, bonded on cracked or corroded metallic aircraft structures, have shown to be a highly cost effective method for extending the service life and maintaining high structural efficiency. An aluminum double lap joint plate was considered as a damaged aircraft structural element in this paper. We repaired the plate with carbon fiber epoxy composite patch by induction curing, and by oven curing method. We also repaired it by precured composite patch bonding method, and by cocured composite patch bonding method. Then, the bond strengths were compared among different processing methods. The technique of electromagnetic induction is able to locally and rapidly heat the area close to the adhesive bond line. This allows for the efficient repair of the metallic substrate of aircraft, and may hence be regarded as a more efficient process. Induction heating constitutes an ideal candidate for supplying the heat needed for curing adhesives and resins, which are used for the fabrication of

reinforcing patches, either on the flat, or over geometrically complex surfaces. We had conducted the experiment and numerical simulation to show that the induction curing was efficient repair heat sources in repairing metallic substrate of aircraft. We also investigated whether the incorporation of carbon nanotubes (CNTs) in the adhesive bondline affected bond strength.

We found that the induction-cured samples exhibited bond strengths similar to those of the corresponding oven-cured samples; this was true for both the baseline and the CNT-reinforced samples. Further, the samples processed using cocured patches exhibited higher bond strengths than did the corresponding samples processed using precured patches. In the case of both the precured and the cocured patch samples, the dispersion of 0.5 wt% CNTs in the adhesive bondline increased bond strength slightly. The effect of the two different types of patches placed on top of the aluminum substrate on the rate of temperature increase by induction curing was shown experimentally. And, numerical simulations were performed in case of the precured patch and un-cured patch on top of the aluminum substrate. The results from this study show that the induction curing and cocuring method may be regarded as a sound and efficient method for composite patch bonding repair.

Keywords: aircraft structure, composite patch repair, induction heating, adhesive, bonded joints, carbon nanotubes

Student Number: 2010-30787

Contents

List of figures

List of tables

Nomenclature

T_0	Longitudinal tension per unit width in the outer adherend
T_i	Longitudinal tension per unit width in the inner adherend
τ	Shear stress
u	Longitudinal displacement
ε	Strain
E	Young's modulus
t	Thickness of the outer adherend
G_a	Shear modulus of adhesive
γ	Shear strain
η	Thickness of the adhesive layer
l	Length of the bonded region
α	Degree of cure
$\frac{d\alpha}{dt}$	Rate of cure
E	Electric field intensity
D	Electric flux density
H	Magnetic field intensity
B	Magnetic flux density
J	Conduction current density
ρ^{charge}	Electric volume charge density
ε	Permittivity
μ	Magnetic permeability

σ	Electrical conductivity
φ	Electric scalar potential
σ_{ind}	Conductivity of coil
T	Temperature
ρ_D	Density
c	Specific heat
k	Thermal conductivity
$\dddot{q}$	Heat source density induced by eddy currents per unit time
h_f	Convection surface heat transfer coefficient
C_s	Radiation heat loss coefficient
ε_s	Emissivity of workpiece
σ_{SB}	Stevan-Boltzmann constant
Q_s	Surface loss
T_s	Surface temperature
T_a	Ambient temperature

Chapter 1

INTRODUCTION

Chapter 1
Introduction

1.1 Overview and problem description

The development of composite materials has led to the creation of a new method for the repair of metallic structures, namely, a method based on the adhesive bonding of composite patches. Bonded patch repair is mechanically efficient and is a cost-effective method for maintaining both military and civil aircraft [1]. Bonded composite patches have been used widely for repairing cracks and defects in aircraft structures in recent years [2]. This technology offers many advantages over mechanical fastening or riveting, including improved fatigue behavior, restored stiffness and strength, reduced corrosion, and ready moldability into complex shapes.

Bonded patch repair is performed by adhesively bonding a patch to the damaged area. Proper curing of the adhesive is critical for ensuring the strength and integrity of the repaired part. Traditionally, the hardening of the adhesive has been performed by placing the joint, and hence the structure to be bonded, in an oven or autoclave until the adhesive is fully cured. An inherent drawback

of this technique is the extremely long periods required for complete curing [3], and the unavoidable simultaneous heating of the metallic substrate with the composite patch. This can have negative effects on the durability of the repair work, because of the stresses induced by the difference in the coefficients of thermal expansion of the metal substrate and the composite patch. Ideally, when bonding a composite to a metal, one should avoid heating the substrate when the composite is being cured. This means that the metal base in contact with the adhesive should be heated to a depth of a few millimeters only [4].

Adhesives with low curing temperatures have been developed for repair applications; however, they require the use of portable heating systems, such as heat lamps or heat blankets, when used for field repairs. In addition, such adhesives are ineffective for repairing thick structures and result in substantial heat loss to the surrounding materials. Electromagnetic induction, on the other hand, can be used to locally and rapidly heat the area close to the adhesive bondline [5]. This allows for the efficient repair of the metallic substrates in aircraft, and hence, may be regarded as a more efficient process than the methods that require heating systems. Induction heating-based techniques allow for greater control over the distribution of heat, which is applied only to the composite patch; further, the metallic base is heated to a very small depth [4]. Recently, significant research has been carried out to adapt induction heating to composites to ensure low cost and reduced processing times. A remotely located induction coil transfers electromagnetic energy to the repair structure, which, in turn, radiates thermal energy in the plane of the bondline. This technique allows

for the rapid heating of the adherends and, through thermal conduction, the rapid heating of the adhesive. In addition, owing to the noncontact nature of induction heating, it may be possible to bond several layers at the same time, resulting in reduced repair times. Conventional heating techniques, such as those involving the use of heat blankets, can only bond one layer at a time.

With the increasing aging aircraft in the Korea Air Force, many unanticipated structural defects have surfaced in aircraft. Many structural repair methods have been developed, but there is a need for a more efficient method than conventional mechanical riveting. The Air Force has previously used the composite patch bonding repair method through oven or heat blanket curing. This technology offers many advantages over mechanical fastening or riveting, including improved fatigue behavior, restored stiffness and strength, reduced corrosion, minimal changes to aerodynamic contours, weight saving, reduced cost and readily formed into complex shapes. It was a reasonable method but we had required more fast, efficient and easily applicable method in field maintenance or combat situation. Repair of such an aircraft structure will require heating locally at the appropriate patch bondline and one such method is induction heating. Induction heating techniques are well known and widely used for metals and alloys. Our research has been undertaken to adapt induction heating to composites patch bonding repair for benefits such as cost and reduced processing times.

A number of researchers have reported the benefits of incorporating carbon nanotubes (CNTs) in polymeric composites. For example, it was found that an

epoxy-based polymer matrix composite exhibited an increase in modulus and strength during both tension and compression after the incorporation of CNTs [6]. However, a common problem encountered when using CNTs is ensuring that they are uniformly dispersion. CNTs have a tendency to attract each other and form agglomerates. In order to overcome this issue, mechanical means of dispersion, such as high-power shear mixing and sonication, have been studied [7]. Further, a recent study investigated the increase in the strength of joints when carbon nanotubes are dispersed along the interface. CNTs can be categorized as being single-, double-, or multiwalled, on the basis of the number of concentric graphene sheets that constitute the individual nanotubes. CNTs have shown promise in improving the mechanical, electrical, and thermal properties of composites in numerous applications [8]. Using these CNT properties, we conducted experiment to enhance composite patch bonding by addition of CNTs because we had needed more strengthening method than conventional composite patch bonding repair method. So we had enhanced the composite bonding repaired structure by the addition of CNTs at bondline.

1.2 Literature review

1.2.1 Composite patch repair and CNT reinforcement

Composite patches, bonded on cracked or corroded metallic aircraft

structures, have shown to be a highly cost effective method for extending the service life and maintaining high structural efficiency. Damage tolerant and fail-safe design of aircraft, aerospace and civil structures requires a substantial amount of inspection and defects-monitoring at regular intervals. There is a large number of high-cost inventory of aircraft structures in operation throughout the world, that are undergoing continuous degradation through aging. Moreover, this number is increasing by around 5% every year, resulting in significant negative impact on the economy of many nations. The degradation of defects critical structures is controlled through careful and expensive regularly scheduled inspections in an effort to reduce their risk of failure.

The replacement of a damaged structural component has a relevant impact on the life cycle cost of an aircraft. Bonded composite patches for repairing cracks and defects in aircraft structures have been widely used in the last years. This technology offers many advantages over mechanical fastening or riveting, including improved fatigue behavior, restored stiffness and strength, reduced corrosion and readily formed into complex shapes. The repair of metal structures with composite materials is a technology that was first introduced in Australia in the early 1970s and later in USA in early 1980s. It is now estimated that over 10000 flying patch repairs, for corrosion and fatigue damages, have been performed on Australian and US military aircraft [9]. This technology was first used for the repair of military aircraft and then applied also to civil aircraft. The success of a bonding repair depends on the properties of both the adhesive

and the patch. The quality of the repair depends upon bonding process and surface treatment as well. Carbon–epoxy composites have been mostly used in aeronautics due to their high stiffness and strength to weight ratios. The performance of the adhesive plays a key role in the successful utilization of bonded composite patch repairs. The role of a bonded composite patch is to restore the stress state modified by the presence of the crack. The stress intensity factor is then reduced by the presence of the patch. Many authors have already investigated the behavior of metallic structures repaired by composite patches.

Schubbe & Mall [10] investigated whether a cracked thick aluminum panel could be repaired with a bonded composite patch. They examined the effects of various patch parameters (i.e., the patch length and patch-to-panel stiffness ratio) related to asymmetric bonded repair on the fatigue behavior of a cracked thick aluminum plate in the unrestricted condition by characterizing the effects of these parameters on the crack growth rate, debonding behavior, and fatigue life. Baker et al. [11] performed repairs on Mirage aircraft using the boron fiber-reinforced plastic (BFRP) crack-patching technique. Baker and Jones studied an aluminum panel repaired with composite patches. For a repaired cracked plate they showed that the stress intensity factor does not increase indefinitely with the crack length, as it asymptotically reaches a limit value [11]. According to Baker's results, Rose showed that the stress intensity factor range of a repaired structure does not depend on the crack length if the crack grows up below the repair [12]. As a result, the crack growth rate does not depend on of crack

length according to the Paris law. Klug [13] investigated the fatigue behavior of pre-cracked 2024-T3 aluminum plates repaired with a bonded carbon/epoxy patch. Single sided repairs were found to provide about a 4-5 times improvement in the fatigue life.

After these early works many authors have addressed many numerical and experimental aspects. Naboulsi, Schubbe and Mall [14] have analyzed the modeling of the composite and adhesive layers, using the three layer technique in comparison with the high computational cost of the three dimensional Finite Element models. Naboulsi and Mall [15] have successively adopted the three layer technique for the nonlinear analysis of the repaired structure in order to take in account large displacements and material nonlinearities. Chung and Yang and Jones [16], Whittingham and Marshall have investigated the fracture and the crack growth behavior in a more complex structure, such as stiffened panel, deriving some design formulas. Cheuk et al [17] had experimental and numerical investigations of the fatigue crack initiation and growth mechanism in metal-to-composite bonded double-lap joints. The paper results suggest that fatigue failure of metal-composite double-lap joints is mainly driven by tensile mode loading due to the peel stress. Some other authors have focused their attention on the optimal design of the bonded patches, by finite element models, in terms of edge taper (Wang et al.) [18] and in-plane shape [19]. Some of the above mentioned numerical activities have been compared with experimental data measured with reference to the stress intensity factor and fatigue life of the repaired structural elements (Schubbe & Mall; Wang et al.) [1, 20].

In addition, a lot of researches have been done about the CNTs. Recent study has addressed the strength enhancement of such a joint using dispersed carbon nanotubes (CNTs) along the interface. CNTs may be categorized as single-, double-, or multi-walled based, on the number of concentric graphene sheets rolled together to make up the nanotube, and have shown promise for improving mechanical, electrical, and thermal properties for many applications [8]. It has also been demonstrated that CNTs, when dispersed along a fully bonded scarf joint interface, could improve the Mode I and Mode II fracture toughnesses of the joint [7]. Burkholder et al. [7] investigated how the addition of various types of CNTs to the adhesive affected the fracture strength during Mode II loading. Srivastava [21] studied the use of C/C and C/C–SiC composites as substrates bonded with thin layers of multiwalled CNTs (MWCNTs) that either contained or did not contain an epoxy resin.

1.2.2 Curing with induction heating

The critical issue in adhesive-based bonding composites patch repair is the application of sufficient heat and consistent pressure at the bondline. It is highly desirable that thermal generation be localized at the bondline and be evenly distributed. This is especially important with the increasing use of multifunctional hybrid composites. Repair of such a thick-section structure will require heating locally at the appropriate patch bondline and one such method is induction heating. In addition, due to the noncontact nature of induction heating,

it may be possible to reduce repair times for the part.

Induction heating techniques are well known and widely used for metals and alloys. Recently, significant research has been undertaken to adapt induction heating to composites for benefits such as cost and reduced processing times. One of the heating techniques uses hysteresis losses in ferromagnetic particles subjected to high frequency magnetic fields as the heat generation mechanism. Another generates heat through Joule losses caused by the formation of eddy currents through Faraday's Law. Both of these heating techniques can be applied to the composites patch repair. The remotely located induction coil transfers electromagnetic energy to the structure, which in turn radiates thermal energy in the plane of the bond-line. These techniques allow rapid heating of the adherends material and, through thermal conduction, rapid heating of the adjacent adhesive. These methods have traditionally been plagued by non-uniformity of heating in the plane of the bond-line. In a recent work, a methodology for relating cure cycles to degree of cure predictions for accelerated curing of adhesives was established. Eddy-current-based susceptors based on electrically conductive meshes and epoxy-based adhesives were used. It has been shown that similar properties are achieved for rapidly induction heated adhesive bonds compared to baselines [3].

A lot of researches have been done to use induction heating for composite curing. Through-thickness heating behavior of carbon fiber-based prepreg stacks, during induction processing, H. J. Kim et al. [22] was investigated with theoretical models for dielectric hysteresis and contact resistance heating

mechanisms. Yarlagadda and Kim et al. [5] focused on the through-thickness heating behavior during the induction processing of carbon fiber-based prepreg lay-ups. Mathur, R. et al. [23] reported a genetic algorithm that can be used as a computationally efficient tool for cut mesh design for the induction bonding process. They successfully had determined optimal cut mesh patterns in the mesh optimization for the induction bonding process. A study of the feasibility of using induction heating as a mean of hardening adhesives in composite bonded joints has been performed by Mahdi [3]. From the research, they found the strength of the joints was however seen to be dependent on the loading mode.

1.3 Research objective and scope

This study focused on the use of adhesive joints (double-lap joints) to bond aluminum–composite sections of interest of aircraft structures; however, the results should be applicable to other types of structures as well. The objectives were to investigate the effects of various bonding parameters on the fracture strength of the formed bond. It should be noted that the data presented in this study allow for both a comparison of different curing methods (oven and induction curing) as well as different fabrication techniques (the use of precured patches or the use of cocured patches). A true comparison of the curing and fabrication methods would have involved a comparison of the strengths of

double-lap adhesive joints. Another aim of the study was to investigate how the addition of CNTs in the adhesive bondline affects the shear strength during tensile loading. This was also determined on the basis of the strengths of the double-lap adhesive joints. The study involved the preparation of five joints for each condition, and testing their shear strengths by increasing the load until failure.

In chapter 2, the management of aging aircraft in the Air Force is presented. Several problems corresponding to aging aircraft have been described therein. A proper repair method is proposed to solve the problems. This method, composite patch bonding, can extend the service life of aging aircraft. We explain the theoretical background for the composite patch-bonding repair and examine induction heating as an efficient heat source in composite patch bonding repair.

In chapter 3, the experimental method and procedures are explained and material properties and the sample schematic are described. The DLS (double lap joints shear) samples provided a means to compare the shear strength of oven-cured samples with that of induction-cured samples. The shear strength of the sample was also compared with the precured patch samples and cocured patch samples. CNTs (carbon nanotubes) were inserted at the bondline in each sample to improve strength. We also investigated how the addition of CNTs in the adhesive bondline affected shear strength in tension loading.

Chapter 4 describes the experiment and numerical simulations. Experiments were performed to check whether the patch (precured patch or cocured patch)

effects the temperature rise rate of the aluminum substrate when curing by induction heating. Using the same conditions as the experiment, numerical simulations were conducted with a commercial program code and were compared to the experimental results. We show that induction heating was an efficient heat source for composite patch repair of metallic aircraft substrates.

Chapter 2

BACKGROUND AND THEORY

Chapter 2
Background and theory

2.1 Management of aging aircraft

2.1.1 Overview of aging aircraft

With the increasing aging aircraft, many unanticipated structural defects have been occurred in aircraft. An aircraft begins to 'age' as soon as it first flies and various effects begin to occur as shown in Figure 2.1. However, the term is usually applied to the issues which can begin to arise as the time-since-new becomes significant and greater than the average age of similar class aircraft. The process of aircraft design and the subsequent establishment of principles for an approvable maintenance program aim to take full account of the effects of continued use of aircraft. Damage Tolerance and Safe Life Design philosophies are applied nowadays and appropriate inspection methods and inspection intervals are developed to identify the effects of accidental, environmental or fatigue damage. It is also now usual for a fatigue-related

sampling inspection program and a corrosion prevention and control program to be established. Keeping older jet aircraft in an airworthy condition has been found to present special difficulties which have not all been addressed by prescribed maintenance. The serious continuing airworthiness issues which have arisen in many ageing aircraft have often been a direct consequence of this gap between current and former practices required for Aircraft Certificate issue and maintenance program approval.

Until quite recently, some significant issues arising from aircraft age have not been recognized and addressed until after fatal accidents have occurred. The Air Force Republic of Korea, which has seen most examples of accidents attributed to aging aircraft problems, has for some interest to coordinate the development of risk management solutions for the various types of aging aircraft problem, especially structures. Awareness of these safety issues in the other leading airworthiness jurisdictions of design, production and maintenance regulation is now similarly high and preventive interventions are being developed. The maintenance issues which have particularly arisen with aging aircraft structural failure have generally been seen as arising from fatigue or corrosion, with corrosion sometimes initiating fatigue effects.

2.1.2 Metallic corrosion

Metallic corrosion occurs when chemical action causes deterioration of the surface of a metal. Most corrosion is galvanic or electrolytic in origin, which means that it has occurred because two dissimilar metals have been together in an electrolyte (usually contaminated water). This effect can also occur at the microscopic grain boundaries within a metal alloy. However it arises, it may go undetected and result in loss of integrity of metallic structures. Prevention in the long term will be by better design and selection of materials, which nowadays include proven non metallic composites. There is also a need for a better understanding of the detailed effects of corrosion on structural integrity. Chronological age is especially relevant to corrosion incidence, as is the ground environment where an aircraft is usually parked as well as the typical flight environment. For existing aircraft, improved inspections, including the use of non-destructive testing (NDT), and the management of any corrosion found through effective repair techniques, mapping technologies, and recording are the main option. However, in either case, better use may be able to be made of corrosion prevention technologies including substitution of alternative materials or the use of coatings or inhibitor treatments. If any corrosion defect occurred on metal structure, repairing by composite patch will be reasonable method.

2.1.3 Structural fatigue

Structural fatigue has produced a number of ageing aircraft losses. An early illustration of the extent to which the controls against fatigue failure introduced during the early years of the 'jet age' might have been inadequate was delivered by a 1988 incident to a 19 year old Boeing 737-200: on an internal flight in Hawaii it suffered sudden structural failure and explosive decompression at FL240. Nearly 6 meters of cabin skin and structure aft of the cabin entrance door and above the passenger floor line separated from the aircraft. The subsequent investigation found de-bonding and fatigue damage which had led to the failure. For that aircraft at least, the introduction of static test hulls with simulated hours and cycles kept well ahead of equivalent in-service aircraft was not sufficient. The aircraft involved had completed 89,680 flight cycles with an average flight time of only 25 minutes, almost all of them in the marine environment of the Hawaiian Islands, a somewhat atypical service life which was considered to have allowed corrosion to increase the likelihood of fatigue. The possibility of structural fatigue from any origin has been actively considered since the advent of pressurized aircraft when there were accidents attributable to an insufficient understanding of some basic design issues. Since then, aircraft design procedures have involved the carefully-researched creation of structures which will withstand a stated number of flight cycles with a low probability that the strength of the structure will degrade below its designed ultimate strength before the end of its approved life. However, sometimes older structures are found to no longer meet their damage tolerance requirements

because repeated cyclic or exceptional ‘G’ loading has unexpectedly produced cracks of a sufficient size and density in a structure to weaken it so much that it no longer has the intended residual strength. This may happen not just in metals but other materials increasingly used in aircraft construction. The only available defense is better detection inspections during base maintenance including the use of NDT. In some cases, this means proper application of existing maintenance procedures, especially in respect of repairs; but in other cases, the specification and oversight of those procedures has been such as to make detection of dangerous levels of structural fatigue unlikely, especially when a direct or indirect consequence of a repair. The mechanism by which fatigue propagates in a structure is the well known crack. Cracks propagate because the geometry of a crack produces a very high concentration of stress at the end of the crack and eventually, if a growing crack goes undetected, fracture will occur. Fatigue cracks have been found to arise in several ways: especially from fastener holes such as those for rivets, bolts, nuts and screws where localized stress concentration can initiate premature cracking. When repairing also, the stress concentration that would be avoided. When repair the cracking by mechanically, there are also have several disadvantages: Stress concentrations at fastener holes, difficult to detect cracks under patch, rapid crack growth on exit from patch, danger of corrosion under patch etc. But repairing by composite patch bonding repair has many advantages: No damage to structure or hidden components, slow crack growth even on exit from patch, high

reinforcing efficiency, can repair cracks, can detect crack growth under patch, no corrosion problems, sealed interface etc.

2.1.4 Maintenance of aging aircraft in Air Force

Any discussion of the wisdom of maintaining aircraft is usually based on economic arguments. For example, if the cost of maintaining the aircraft on a monthly or annualized basis exceeds the capital, interest, and amortization charges on replacement equipment, the decision to purchase the replacement is straightforward. In the case of Air Force aircraft, safety of flight considerations also enters into the decision to repair or replace. Fortunately, inspection and maintenance procedures and the ASIP (Aircraft Structural Integrity Program) have been developed to reduce the likelihood of structural failure during the design service life. So Air Force managers have concluded that the only way to meet mission demands is to extend the service life of some of their aircraft forces. The extended use of many aircraft results in increased maintenance and repair costs because of structural cracking and corrosion problems. In most cases, older aircraft spend longer times undergoing depot maintenance, with a resulting severe impact on readiness. Furthermore, extended aircraft service places increased importance on forecasting when the system must be replaced, either because of obsolescence or economic reasons. If a system must be retired before the expected forecast service life, readiness could be impacted severely

because a replacement system would not be ready in time to close the gap. Extended production lead times and budget exigencies for new systems make it even more important that the Air Force accurately determine, with a high degree of precision and confidence, the expected structural life of aircraft system and the economics of sustaining them.

An effective airframe structural maintenance program evaluates sources of structural deterioration. When structural deterioration is detected in the maintenance program, a decision must be made to either repair or replace the affected components. The primary damage mechanisms is to be considered for aging aircraft include corrosion, SCC (stress corrosion cracking), low/high cycle fatigue. In the case of corrosion, the primary issue involved in the restoration of corroded structure is the removal and reapplication of protective finishes to prevent further corrosion.

Repair of damage resulting from in service degradation mechanisms such as fatigue, SCC, corrosion, and discrete source damage (e.g., foreign object impact, handling damage, lightning attachment) is a critical maintenance activity. Generally, repair of aged structure consists of reinforcement doublers that are bolted or bonded over the damaged area. Bolted repairs are generally preferred for commercial aircraft because they are relatively simple to perform and minimize the time that the aircraft is out of service. However, bolted repairs introduce stress concentrations at fastener holes and tend to add considerable weight. Recent Air Force efforts have emphasized bonded composite patch

repairs, even though the repairs are more complex and time consuming to design and install. Bonded repairs avoid stress concentrations from drilled holes, are more readily conformable to complex shapes, and provide more efficient load transfer at lower weight compared with bolted repairs. The primary technical issues for structural repairs include; analysis methods and design practices for repairs; material and process selection and optimization, including surface preparation, lamination, and bonding processes, and specification infrastructure for bonded repairs; life prediction and inspection intervals for the repaired structure; maintaining the damage tolerance of the repaired structure [24].

Another important issue in the maintenance of aging systems is the replacement of components that are fabricated using alloys and processes that are susceptible to deterioration, especially corrosion and SCC. Improvements in commercial alloys, tempers, process controls, and fabrication methods could be beneficial if guidelines were provided to the logistic centers for materials and process substitution decisions including performance and cost tradeoffs. Commercial airframe manufacturers have been active in updating obsolete materials and process specifications in their core design and manufacturing practices and in their maintenance programs.

2.1.5 Repairing of aircraft at ABDR

During times of conflict rapid repairs are required to keep aircraft operational with a useful level of mission capability, or to return them safely to a depot for major maintenance if acceptable mission capability cannot be restored. This technology, known as Aircraft Battle Damage Repair (ABDR), maximizes aircraft availability so can prove to be a decisive factor in times of conflict. During peacetime the technology is also relevant as aircraft can sustain damage at remote locations where full depot facilities are unavailable. In such cases, there is a requirement to perform temporary repairs with minimum equipment so that the aircraft can be flown back to a depot [25].

ABDR must restore the aircraft to as near original design static strength and capability that the time, equipment and personnel constraints imposed by the operational situation allow. Battle damage repairs are undertaken at forward operational bases or under field conditions without access to full workshop facilities. At present conventional ABDR is based on the use of metallic, mechanically fastened patches. However, since such repairs require the introduction of many new fastener holes the component is made more difficult to repair permanently later and may need to be replaced. Bonded composite repairs, in contrast, do not damage the component, since fastener holes are not required and, unlike metallic repairs, composites are highly formable so can readily be applied to complex contours. Early several experimental showed that bonded composite ABDR performed better than traditional mechanically fastened metallic repairs when loaded in both static and fatigue [26].

2.2 Overview of patch repair

2.2.1 Properties of patching technology

Excellent load transfer characteristics bonded reinforcements or patches provide a stiff alternative load path so they can be used very effectively to repair live cracks as shown in Figure 2.2. In contrast, standard repairs as shown in Figure 2.3, based on mechanically fastened metallic patches provide a relatively compliant alternative load path so they cannot effectively repair cracks and require prior removal (or some other terminating treatment) of the cracked region. Mechanical repairs also have several other disadvantages, compared to bonded repairs [27]. The high-performance fiber-composites boron/epoxy and graphite/epoxy are highly suited for use as a patching or reinforcing material for defective or degraded metallic structure. Briefly the attributes of these composites include: High Young's modulus and strength, which minimizes the required patch thickness; Highly resistant to damage by cyclic loads; Immunity to corrosion, forms excellent protective layer; High formability, which allows easy formation of complex shapes; Low electrical conductivity (boron/epoxy only), which facilitates use of eddy current NDI for monitoring the patched cracks and eliminates concerns with galvanic corrosion. The main disadvantage of composites as patching materials results from their relatively low coefficient of thermal expansion compared to the parent material

which results in residual tensile mean stresses in the repaired component. Although relatively costly, boron/epoxy is chosen as the patch or reinforcement for most Australian bonded composite repair applications, mainly because of its excellent mechanical properties, low conductivity and relatively high coefficient of thermal expansion. However, graphite/epoxy because of its better formability is chosen for regions with small radii of curvature and sometimes because of its low cost and much higher availability. Patches are generally bonded with an aerospace-grade structural epoxy-nitrile adhesives, curing from 80°C to 120°C to provide a maximum temperature capability of around 100°C. Composite reinforcement can be used for a wide range of repairs/ reinforcements to metallic aircraft components, many of which have been successfully exploited in Australia.

2.2.2 Double-lap joint

The geometric profile of a double-lap joint is shown in Figure 2.4. The free-body-diagram of an infinitesimal element in the overlap region is shown in Figure 2.5. The force equilibrium of upper and lower adherend in Figure 2.4 yields to the following differential [28]:

$$\frac{dT_0}{dx} + \tau = 0 \tag{2-1a}$$

$$\frac{dT_i}{dx} - 2\tau = 0 \tag{2-1b}$$

where T_0, T in equations (2-1a) and (2-1b) represents longitudinal tension per unit width in the upper and lower adherend, respectively, τ is the shear stress in the adhesive layer.

The longitudinal displacement-strain relations of adherends are:

$$\frac{du_0}{dx} = \varepsilon_0 = \frac{T_0}{E_0 t_0} \tag{2-2a}$$

$$\frac{du_i}{dx} = \varepsilon_i = \frac{T_i}{E_i t_i} \tag{2-2b}$$

where u_0, ε_0, E_0 and t_0 are the longitudinal displacement, strain, Young's modulus, and thickness of the outer adherend, respectively. u_i, ε_i, E_i and t_i are the respective components relative to the inner adherend. The differential equations (2-1a) and (2-1b) can be combined together through the shear deformation in the adhesive layer as follows:

$$\tau = G_a \gamma = \frac{G_a}{\eta}(u_i - u_0) \tag{2-3}$$

where G_a is the shear modulus of adhesive, γ and η are the shear strain and thickness of the adhesive layer, respectively.

Taking the derivative with respect to x of equation (2-3) and equation (2-1a), yields

$$\frac{d\tau}{dx} = \frac{G_a}{\eta}\left(\frac{du_i}{dx} - \frac{du_0}{dx}\right) \tag{2-4}$$

$$\frac{d^2T_0}{dx^2} = -\frac{d\tau}{dx} \tag{2-5}$$

Substituting equation (2-4) and equation (2-2a) and (2b) into equation (2-5) yields

$$\frac{d^2T_0}{dx^2} = -\frac{G_a}{\eta}\left(\frac{du_i}{dx} - \frac{du_0}{dx}\right) = -\frac{G_a}{\eta}\left(\frac{T_i}{E_iT_i} - \frac{T_0}{E_0T_0}\right) \tag{2-6}$$

The force balance requires that the sum of longitudinal forces in outer and inner adherend equals to the applied force P, i.e.

$$P = T_i + 2T_0 \quad \text{or} \quad T_i = P - 2T_0 \tag{2-7}$$

Substituting equation (2-7) into (2-6), one can obtain a second-order differential equation of T_0 with respect to x as follows:

$$\frac{d^2T_0}{dx^2} - \lambda^2 T_0 = -\frac{G_a P}{E_i t_i \eta} \tag{2-8}$$

Where,

$$\lambda^2 = \frac{G_a}{\eta}\left(\frac{2}{E_iT_i} - \frac{1}{E_0T_0}\right)$$

The associated boundary conditions are

$$T_0 = 0, \quad x = \frac{l}{2}$$

$$T_0 = \frac{P}{2}, \quad x = -\frac{l}{2} \tag{2-9}$$

where l is the length of the bonded region.

The solution of differential equation (2-8) can be written as

$$T_0 = A\sinh(\lambda x) + B\cos(\lambda x) + \frac{PE_0t_0}{(2E_0t_0 + E_it_i)} \tag{2-10}$$

The integration constants A and B can be solved by applying the boundary conditions in equation (2-9). As a result, the longitudinal tensions, T_0 and T_i, in outer and inner adherend and the shear stress τ in the adhesive layer can be expressed as the following forms:

$$T_0 = \frac{p}{2}\left[-\frac{1}{2}\frac{\sinh(\lambda x)}{2\sinh\left(\frac{\lambda l}{2}\right)} + \frac{E_it_i - 2E_0t_0}{2(E_it_i + 2E_0t_0)}\frac{\cosh(\lambda x)}{\cosh\left(\frac{\lambda l}{2}\right)} + \frac{2E_0t_0}{E_it_i + 2E_0t_0}\right] \tag{2-11}$$

$$T_i = p\left[1 + \frac{1}{2}\frac{\sinh(\lambda x)}{2\sinh\left(\frac{\lambda l}{2}\right)} - \frac{E_it_i - 2E_0t_0}{2(E_it_i + 2E_0t_0)}\frac{\cosh(\lambda x)}{\cosh\left(\frac{\lambda l}{2}\right)} - \frac{2E_0t_0}{E_it_i + 2E_0t_0}\right] \tag{2-12}$$

$$\tau = \frac{p\lambda}{4}\left[\frac{\cosh(\lambda x)}{\sinh\left(\frac{\lambda l}{2}\right)} - \frac{E_it_i - 2E_0t_0}{2(E_it_i + 2E_0t_0)}\frac{\sinh(\lambda x)}{\cosh\left(\frac{\lambda l}{2}\right)}\right] \tag{2-13}$$

The constants E_i and E_0 are the equivalent longitudinal modulus in inner and outer adherends, respectively [28, 29]

2.3 Overview of induction heating

2.3.1 Theory of heating by induction

Induction heating is a non-contact heating process. It uses high frequency

electricity to heat materials that are electrically conductive [30]. Since it is non-contact, the heating process does not contaminate the material being heated. It is also very efficient since the heat is actually generated inside the work-piece. This can be contrasted with other heating methods where heat is generated in a flame or heating element, which is then applied to the work-piece.

A source of high frequency electricity is used to drive a large alternating current through a coil [31]. This coil is known as the work coil. The passage of current through this coil generates a very intense and rapidly changing magnetic field in the space within the work coil. The work-piece to be heated is placed within this intense alternating magnetic field [32]. The alternating magnetic field induces a current flow in the conductive work-piece. The arrangement of the work coil and the work-piece can be thought of as an electrical transformer. The work coil is like the primary where electrical energy is fed in, and the work-piece is like a single turn secondary that is short-circuited. This causes tremendous currents to flow through the work-piece. These are known as eddy currents. In addition to this, the high frequency used in induction heating applications gives rise to a phenomenon called skin effect [30] [32]. This skin effect forces the alternating current to flow in a thin layer towards the surface of the work-piece. The skin effect increases the effective resistance of the metal to the passage of the large current. Therefore it greatly increases the heating effect caused by the current induced in the work-piece. The principle of induction heating is mainly based on two well-known physical phenomena [33].

The development of high-frequency induction power supplies provided a means of using induction heating for surface hardening. The early use of induction involved trial and error with built-up personal knowledge of specific applications, but a lack of understanding of the basic principles. Throughout the years the understanding of the basic principles has been expanded, extending currently into computer modeling of heating applications and processes. Knowledge of these basic theories of induction heating helps to understand the application of induction heating as applied to induction heat treating. Induction heating occurs due to electromagnetic force fields producing an electrical current in a part. The parts heat due to the resistance to the flow of this electric current [34].

2.3.2 Resistance

All metals conduct electricity, while offering resistance to the flow of this electricity. The resistance to this flow of current causes losses in power that show up in the form of heat. This is because, according to the law of conservation of energy, energy is transformed from one form to another-not lost. The losses produced by resistance are based upon the basic electrical formula: $P= i^2R$, where i is the amount of current, and R is the resistance. Because the amount of loss is proportional to the square of the current, doubling the current significantly increases the losses (or heat) produced. Some metals, such as

silver and copper, have very low resistance and, consequently, are very good conductors. Silver is expensive and is not ordinarily used for electrical wire (although there was some induction heaters built in World War II that had silver wiring because of the copper shortage). Copper wires are used to carry electricity through power lines because of the low heat losses during transmission. Other metals, such as steel, have high resistance to an electric current, so that when an electric current is passed through steel, substantial heat is produced. The steel heating coil on top of an electric stove is an example of heating due to the resistance to the flow of the household, 60 Hz electric current. In a similar manner, the heat produced in a part in an induction coil is due to the electrical current circulating in the part [34].

2.3.3 Alternating current and electromagnetism

Induction heaters are used to provide alternating electric current to an electric coil (the induction coil). The induction coil becomes the electrical (heat) source that induces an electrical current into the metal part to be heated (called the work-piece). No contact is required between the work-piece and the induction coil as the heat source, and the heat is restricted to localized areas or surface zones immediately adjacent to the coil. This is because the alternating current (ac) in an induction coil has an invisible force field (electromagnetic, or flux) around it. When the induction coil is placed next to or around a work-piece, the

lines of force concentrate in the air gap between the coil and the work-piece. The induction coil actually functions as a transformer primary, with the work-piece to be heated becoming the transformer secondary. The force field surrounding the induction coil induces an equal and opposing electric current in the work-piece, with the work-piece then heating due to the resistance to the flow of this induced electric current. The rate of heating of the work-piece is dependent on the frequency of the induced current, the intensity of the induced current, the specific heat of the material, the magnetic permeability of the material, and the resistance of the material to the flow of current. Figure 2.6 shows an induction coil with the magnetic fields and induced currents produced by several coils. The induced currents are sometimes referred to as *eddy-currents*, with the highest intensity current being produced within the area of the intense magnetic fields [34].

Induction heat treating involves heating a work-piece from room temperature to a higher temperature, such as is required for induction tempering or induction austenitizing. The rates and efficiencies of heating depend upon the physical properties of the work-pieces as they are being heated. These properties are temperature dependent, and the specific heat, magnetic permeability, and resistivity of metals change with temperature. Figure 2.7 shows the change in specific heat (ability to absorb heat) with temperature for various materials. Steel has the ability to absorb more heat as temperature increases. This means that more energy is required to heat steel when it is hot than when it is cold.

Table 2-1 shows the difference in resistivity at room temperature between copper and steel with steel showing about ten times higher resistance than copper. At 760 °C (1400 °F) steel exhibits an increase in resistivity of about ten times larger than when at room temperature. Finally, the magnetic permeability of steel is high at room temperature, but at the Curie temperature, just above 760 °C (1400 °F), steels become nonmagnetic with the effect that the permeability becomes the same as air.

2.3.4 Hysteresis

Hysteresis losses occur only in magnetic materials such as steel, nickel, and a few other metals. As magnetic parts are being heated, such as those made from carbon steels, by induction from room temperature, the alternating magnetic flux field causes the magnetic dipoles of the material to oscillate as the magnetic poles change their polar orientation every cycle. This oscillation is called hysteresis, and a minor amount of heat is produced due to the friction produced when the dipoles oscillate. When steels are heated above Curie temperature they become nonmagnetic, and hysteresis ceases. Because the steel is nonmagnetic, no reversal of dipoles can occur. Figure 2.8 shows an illustration of hysteresis and the effect on the magnetic flux field strength [34].

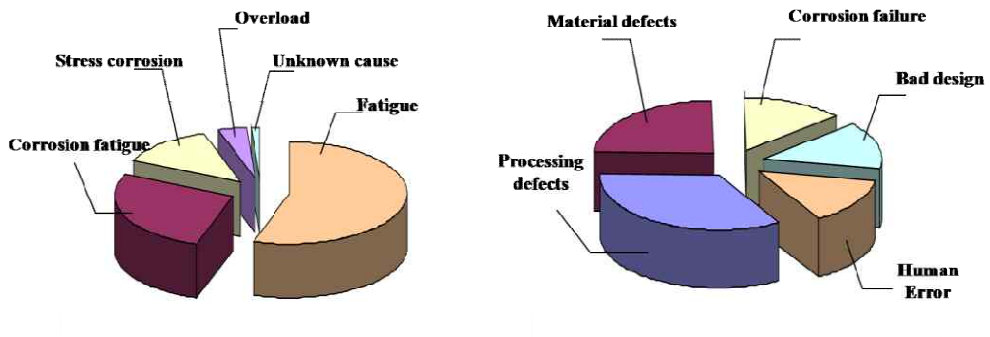

(a) Mechanical failure type **(b) Cause of failure**

Figure 2.1 Failure type of aging aircraft in Korea Air Force

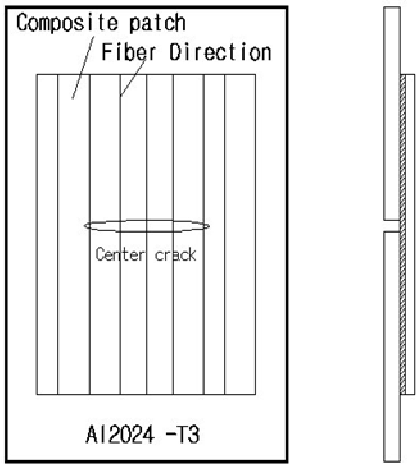

Figure 2.2 Patch bonding repair

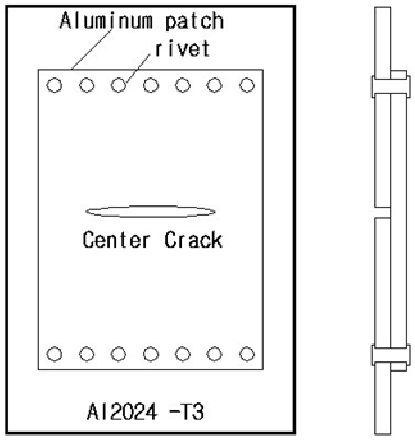

Figure 2.3 Standard repair (mechanically fastened)

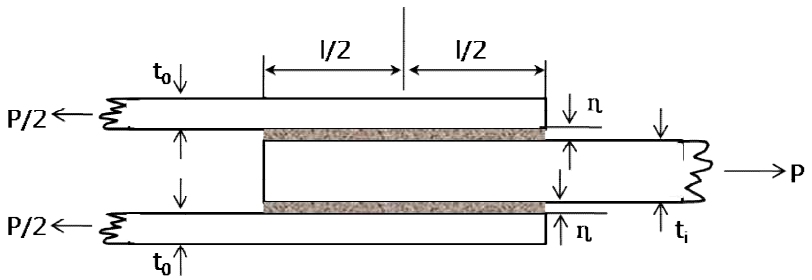

Figure 2.4 Geometric schematic of a double lap joint

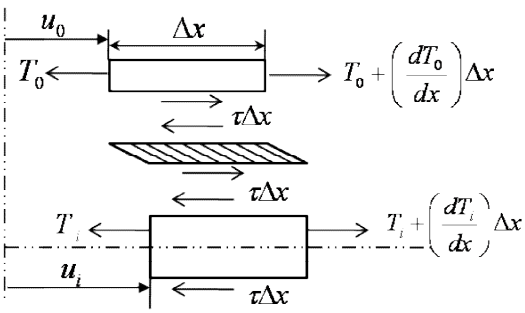

Figure 2.5 Free-body diagram of a double lap joint

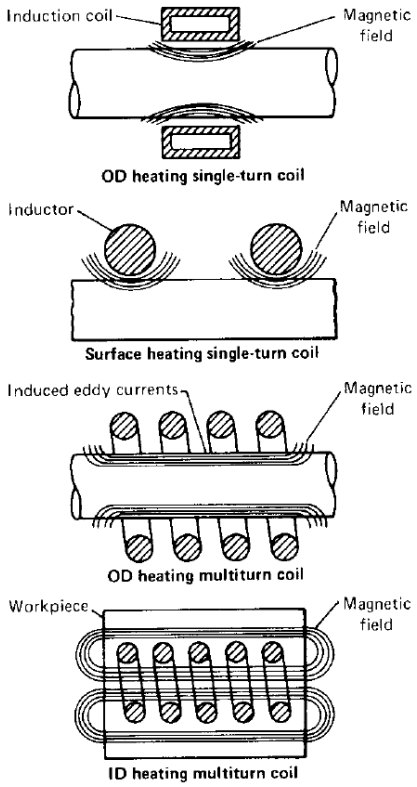

Figure 2.6 Induction coil with electromagnetic field

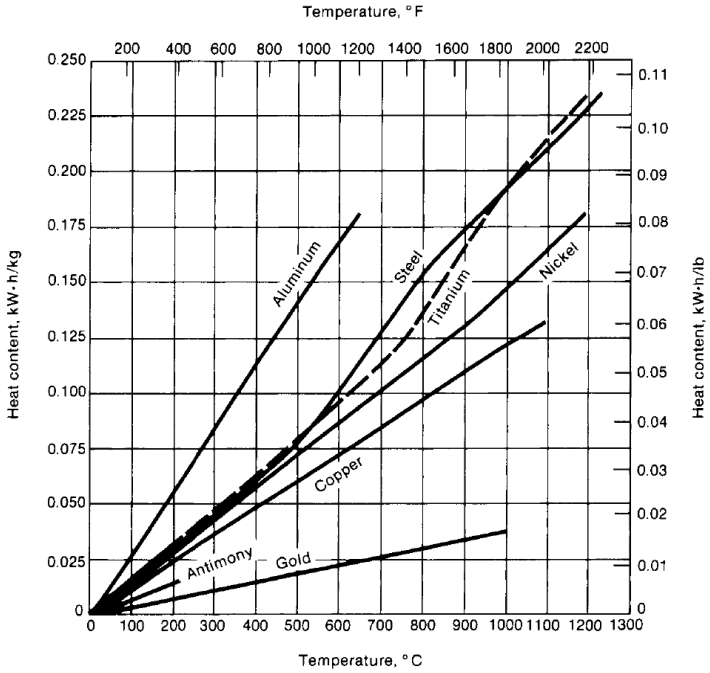

Figure 2.7 Change in specific heat with temperature for materials

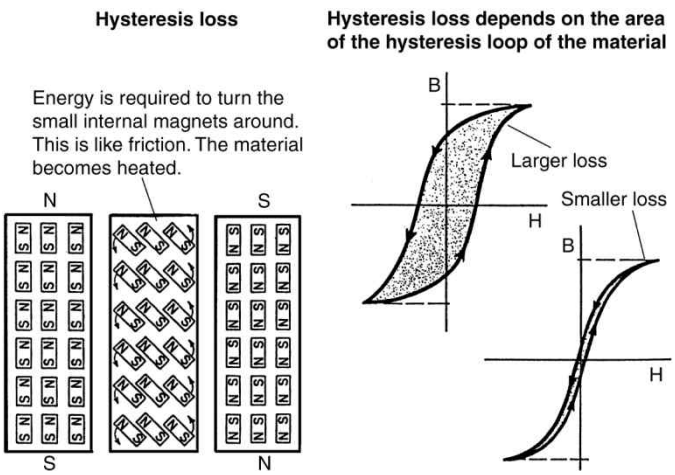

Figure 2.8 Effect of hysteresis on heating rate

Table 2.1 Resistivity of different metals

Material	Approximate electrical resistivity, μΩ · cm (μΩ · in.), at temperature, °C (°F), of:							
	20 (68)	95 (200)	205 (400)	315 (600)	540 (1000)	760 (1400)	980 (1800)	1205 (2200)
Aluminum	2.8 (1.12)	...	...	6.9 (2.7)	10.4 (4.1)	...	...	...
Antimony	39.4 (15.5)	...	...	...	...	...	...	...
Beryllium	6.1 (2.47)	...	...	...	11.4 (4.5)	...	...	...
Brass(70Cu-30Zn)	6.3 (2.4)	...	...	...	...	...	...	...
Carbon	3353 (1320.0)	...	...	...	1828.8 (720.0)	...	...	...
Chromium	12.7 (5.0)	...	...	...	...	...	...	...
Copper	1.7 (0.68)	...	...	3.8 (1.5)	5.5 (2.15)	...	9.4 (3.7)	...
Gold	2.4 (0.95)	...	...	...	...	...	12.2 (4.8)	...
Iron	10.2 (4.0)	14.0 (5.5)	...	...	63.5 (25.0)	106.7 (42.0)	123.2 (48.5)	...
Lead	20.8 (8.2)	27.4 (10.8)	...	49.8 (19.6)	...	...	...	...
Magnesium	4.5 (1.76)	...	...	...	...	...	...	...
Manganese	185 (73.0)	...	...	...	...	...	...	...
Mercury	9.7 (3.8)	...	...	...	...	...	...	...
Molybdenum	5.3 (2.1)	...	...	...	...	...	...	33.0 (13.0)
Monel	44.2 (17.4)	...	...	...	...	...	...	...
Nichrome	108.0 (42.5)	...	...	114.3 (45.0)	...	114.3 (45.0)	...	...
Nickel	6.9 (2.7)	...	...	29.2 (11.5)	40.4 (15.9)	...	54.4 (21.4)	...
Platinum	9.9 (3.9)	...	...	...	...	...	...	...
Silver	1.59 (0.626)	...	...	...	...	6.7 (2.65)	...	...
Stainless steel, nonmagnetic	73.7 (29.0)	...	...	99.1 (39.0)	...	...	130.8 (51.5)	...
Stainless steel 410	62.2 (24.5)	...	...	...	101.6 (40.0)	...	127 (50.0)	...
Steel, low carbon	12.7 (5.0)	16.5 (6.5)	...	...	59.7 (23.5)	102 (40.0)	115.6 (45.5)	121.9 (48.0)
Steel, 1.0% C	18.8 (7.4)	22.9 (9.0)	...	...	69.9 (27.5)	108 (42.5)	121.9 (48.0)	127.0 (50.0)
Tin	11.4 (4.5)	...	20.3 (8.0)	...	...	...	...	...
Titanium	53.3 (21.0)	...	...	...	...	...	...	165.1 (65.0)
Tungsten	5.6 (2.2)	...	...	...	...	...	...	38.6 (15.2)
Uranium	32.0 (12.6)	...	...	...	...	...	...	...
Zirconium	40.6 (16.0)	...	...	...	...	...	...	...

Source: Ref 3

Chapter 3

EXPERIMENT

Chapter 3
Experiment

3.1 Introduction

Adhesively bonded double-lap joint shear (DLS) samples were manufactured using two different curing methods: conventional oven curing and induction curing. The bonding shear strengths of the oven-cured samples were compared with those of the induction-cured ones. In addition, two different types of patches were used in the DLS samples: precured carbon composite patches and uncured prepreg laminate patches that were cocured with the adhesive. The bonding shear strengths of the precured patch samples and the cocured patch samples were also compared. CNTs were incorporated in each sample type at the bondline to improve the bonding strength. The materials, sample preparation procedures, and test methods used in the study are described in this section.

3.2 Experimental preparation

3.2.1 Specimen schematic and materials

The adhesively bonded DLS samples were fabricated using a film-type adhesive, as illustrated in Figure 3.1. The samples consisted of a composite patch bonded to flat Al-6061-T6 aluminum substrates using a single ply of AF-163-2K adhesive film (3M, Scotch Weld, US). The height, width, and thickness of the Al-6061-T6 aluminum alloy plates were 110 mm, 25.4 mm, and 3 mm, respectively. Two aluminum alloy plates were bonded together through a butt joint with the adhesive film and composite patches. The patches consisted of eight layers of the carbon-epoxy prepreg laminate ($[0]_8$) UN200NS (Hankook Carbon Inc., Korea). The planar dimensions of the patch and the adhesive film were 25.4 mm × 25.4 mm, and their thicknesses were 1.6 mm and 0.24 mm, respectively. The material properties of used experiment is described Table 3-1. Two types of patches were prepared. The first type were precured patches, which consisted of 8 layers of a carbon-epoxy prepreg laminate cured using a hot press for 90 min at 120 ºC. The 25.4 mm × 25.4 mm precured patches were machined from a 270 mm × 270 mm cured plate. The second type of patches were cocured patches, which consisted of the uncured prepreg material used for the precured patch, and were to be cocured along with the adhesive. The fiber orientation of the patches coincided with the loading direction.

3.2.2 DSC analysis of film adhesives used in experiment

3.2.2.1 Thermo chemical analysis

In order to maximize the benefits of accelerated cure of adhesives using induction heating a process window must be established for the adhesives of interest. The process window would then be used to optimize the bonding process in terms of time and temperature. Issues which dictate the process window include cure kinetics, evolution of exotherms, flow and wetting, and thermally induced residual stresses. Adhesive cure is the most dominant of these issues and must be addressed to determine cure time as a function of temperature as well as ultimate degree of cure. In this paragraph we have chosen a typical room temperature curing epoxy adhesive film (AF-163-2K) for evaluation of accelerated cure properties.

3.2.2.2 Cure-kinetics model

DSC (Differential Scanning Calorimetry) has been widely used to characterize the cure kinetics of thermosetting polymers including epoxies, polyesters, vinyl esters, and bismaleimides. Since the heat evolution dQ/dt measured by the DSC results from the chemical cross-linking reaction, it is possible to relate the heat evolution (dQ/dt) to the rate of conversion ($d\alpha/dt$) and the conversion (α). This can be accomplished by the following relationships.

$$\frac{d\alpha}{dt} = \frac{1}{\triangle H_{tot}}\left(\frac{dQ}{dt}\right)_t \tag{3-1}$$

$$\alpha = \frac{1}{\triangle H_{tot}}\int_{t_0}^{t}\left(\frac{dQ}{dt}\right)_t dt \tag{3-2}$$

Where ΔH_{tot} is the total heat of reaction, generally determined by averaging the reaction exotherms measured from several dynamic temperature DSC runs. Various chemical kinetic models can then be fit using data which is obtained from isothermal DSC experiments.

The mechanistic models of thermoset cure that usually provide a more accurate representation of cross-linking reactions are not generally applicable to complex systems such as formulated adhesives. There are several empirical models have been successfully used to predict to cure of thermosetting polymers. One popular model was proposed by Kamal and Sourour [35]. This model has found wide spread acceptance for a number of cross-linking reactions and will be used to fit the adhesive studied here:

$$\frac{d\alpha}{dt} = (A_1 e^{-\frac{E_1}{RT}} + A_2 e^{-\frac{E_2}{RT}} \cdot \alpha^m) \cdot (1-\alpha)^n \tag{3-3}$$

In this expression, α is the degree of conversion, and m and n are temperature dependent kinetic constants usually assumed to sum to 2, but often allowed to vary freely. E is the activation energy, R is the universal gas constant, and T is

the absolute temperature in degree Kelvin. By performing a series of isothermal cures, values for the model parameters can be determined and used to predict the cure kinetics of the adhesive. Cure kinetics was characterized with experimental data and kinetic model by curve fitting. DSC heat flow of AF-163-2k film adhesive results are depicted in Figure 3.2. And modeling of cure kinetics was carried out by curve fitting as showed in Figure 3.3. There are (equation (3-3)) six fitting parameter A_1, A_2, E_1, E_2, m, n. The commercial program Matlab was used for the curve fitting. A_1, A_2, E_1, E_2, m, n values are summarized in Table 3-2. The use of the model will enable prediction of the entire curing process over a wide range of processing temperatures. Initially, however, the prediction of cure time at a specific temperature is of greatest interest to apply induction and oven techniques to accelerate adhesive cure.

3.3 Experimental procedure and equipment

3.3.1 Surfaces preparation

The surfaces of the aluminum substrates were subjected to a complex preparation procedure, in order to ensure strong adhesion. The procedure was performed in several stages and included mechanical preparation and chemical activation. The surfaces were initially cleaned with reagent-grade acetone to

remove grease and organic build up. The next step consisted of removing the aluminum oxide layer from the surfaces by abrasion with 220-grit sandpaper. The surfaces were wiped with a lint-free rag to remove any remaining debris. The exposed surfaces were rinsed in acetone, air dried, and cleaned with methyl ethyl ketone (MEK). Then, silane, used as a coupling agent, was applied immediately to minimize surface oxidation. Finally, the silane-treated surfaces were dried with hot air for 10 min. The precured patch surfaces were treated in the same manner as the aluminum substrates.

3.3.2 Baseline sample

The baseline samples were processed as per the following series of steps. First, a single layer of the AF-163-2K adhesive film was placed on both sides of the aluminum substrate after its surfaces had been treated. Then, either a precured composite patch or an uncured prepreg patch, which was to be cocured with the adhesive, was placed on top of the adhesive film. Each sample was respectively cured at conventional oven and induction curing with vacuum bagging as shown in Figure 3.4.

3.3.3 CNT reinforced sample

The benefits of CNT-reinforced polymers have been documented on several occasions. For example, an epoxy-based polymer matrix composite recorded an

increase in modulus and strength, in both tension and compression [6]. However, a common problem encountered in applications requiring dispersed CNTs is ensuring their uniform dispersion. CNTs have a tendency to attract each other, and become clustered. In order to overcome this tendency, mechanical means of dispersion, such as high shear mixing and sonication, have been studied for nanocomposites [7].

3.3.3.1 Dispersion process

MWCNTs (CM-150, Hanwha-Nanotech, Korea) were used in this study. The CNTs had a diameter of 10–15 nm and length of 25–35 μm. To disperse the CNTs in the epoxy resin (KFR 130, Kookdo Chemical Inc., Korea), the epoxy was dissolved in acetone, and the CNTs were mixed and dispersed in it using an ultrasonicator (CV 505 power supply and a CV 33 convertor, Sonics & Materials Inc., US). The solvent was then evaporated in an ultrasonication bath (SD-D300H, SeongDong, Korea) to maintain the dispersed state. Finally, the suspension was placed in a convection oven for 1 h at 50 °C to evaporate the solvent completely. Figure 3.5 shows the CNT dispersion process.

3.3.3.2 Lay up procedure

As was the case for the baseline samples, the CNT-reinforced samples were also fabricated using precured and cocured patches. The only difference, as

mentioned previously, was that dispersed CNTs were applied along the joint interface to strengthen the bondline in the case of the reinforced samples as shown in Figure 3.6. The CNT-containing epoxy was mixed with the hardener (KFR140, Kookdo Chemical Inc., Korea) in a weight ratio of 10:3. The mixed solution was stirred by hand in a plastic cup to a consistent color and smooth texture; this took approximately 3 min. The mixed solution was applied to both sides of the adhesive surface layer using a plastic knife. Approximately 0.13 g of the mixed solution was used for each sample. The CNT-reinforced samples were processed by the same method as that used for the baseline samples; the only difference was the insertion of the CNTs in the bondline in the case of the former.

3.3.4 Curing procedures

The oven and induction curing procedures used to harden the adhesive and the cocured patch are discussed in this section. In each case, the vacuum was consolidated to ensure the uniformity of the applied pressure in order to achieve a constant adhesive bondline thickness. Pieces of peel ply, breather cloth, and vacuum bagging material were placed on top of the stack, which was sealed on all the four edges with sealing tape. The air was suctioned to create a vacuum, and, depending on the sample type, either the adhesive or the cocured patch was hardened. The lay-up of the samples is shown schematically in Figure 3.4. Each sample was cured either in a conventional oven or by an induction curing

method after being vacuum bagged.

3.3.4.1 Oven curing

In the conventional oven curing technique, the vacuum-bagged assemblies of the DLS samples were prepared as per the procedure mentioned above. On the basis of the manufacturers' recommendations for the adhesive and the prepreg laminate, the samples were cured at a temperature of 120 ºC for 90 min cycles as shown in Figure 3.7. The cured panels were subsequently cut into five test samples using a water jet cutter.

3.3.4.2 Induction curing

A 3 kW induction heating unit (WI-340, DIK Co., Korea, as shown in Figure 3.8) was used in this study. It consisted of an alternating current (AC) power supply and an induction coil. The induction heating unit was capable of generating a peak-to-peak current of 0–70 A in the frequency range of 135–400 kHz. The power delivered to the coil was controlled with a 0–100 graded control. The power supply sent an alternating current through the coil, generating a magnetic field. The remotely located induction coil transferred electromagnetic energy to the aluminum substrate, which in turn, heated the aluminum substrate. The adhesive was heated by the conduction of heat energy from the rapidly heated aluminum substrate. A 5-turn circular coil was used for

curing the samples. A temperature sensor was connected to the induction heating system to maintain the substrate at a set temperature. Thermocouples, which measure temperature on the basis of an electromotive force, cannot be used with induction heating systems since the eddy currents generated in such systems can disturb the electrical sensing circuits of the thermocouples. Hence, we used a thermistor-based temperature sensor, as it is not affected by eddy currents.

The induction-cured samples were also prepared as per the procedure described above. After the preparation of the samples, the induction coil was placed above the vacuum-bagged assembly. It should be noted that the distance between the induction coil and the stack is of great importance, as it allows one to control the maximum temperature to which the assembly is subjected. The induction coil was placed 11 mm above the vacuum-bagged assembly. The temperature sensor placed on the substrate allowed the temperature in the vicinity of the bondline to be monitored. The temperature data were fed back to the power controller, which reduced or increased the power to maintain the temperature at 120 °C for 90 min curing cycle as shown in Figure 3.7. The detected bondline temperatures were always slightly higher than the substrate surface temperature, owing to conduction effects; however, the two temperatures were not significantly different, once the steady-state point was reached. The cured panels were subsequently cut into five test samples using a water jet cutter.

3.3.5 Bond strength measurement

DLS samples, shown in Figure 3.1, are well suited for testing adhesively bonded joints. The prepared samples were tested using a universal testing machine (Instron 810 with a 150 kN load cell, shown in Figure 3.9) to determine the bond shear strengths of the various joints. Five samples were tested for each case. The samples were evaluated using the double-lap shear method in accordance with the ASTM D3528 standard for testing the strengths of adhesive DLS samples through tensile loading. All the measurements were performed at ambient temperature.

3.4 Bond strength results and discussion

3.4.1 Baseline sample

The samples without CNTs were tested as described in the “tensile test method”, to ensure failures occurred through the bonding layer. Five samples were tested. Table 3.3 shows the results of the bonding shear strength tests; the standard deviations of the data are shown as well. The average failure strength for each group is shown in Figure 3.10. The error bars in this figure represent the standard deviation values of the experimental data. It can be seen from Table 3.3 that the standard deviation was relatively low for all the samples. The

maximum coefficient of variation is only 4.9% for the induction/cocured samples.

As can be seen from Figure 3.10, the data presented in this study allows for a comparison between the different curing methods as well as between the different patch fabrication methods. With respect to the curing methods, the bond strengths of the oven/precured patch samples and those of the induction/precured patch samples were almost similar, while the bond strengths of the oven/cocured patch samples were 8% higher than those of the induction/cocured patch samples. On the other hand, with respect to the patch fabrication methods, the cocured patch samples cured using oven and induction heating exhibited bond strengths 18% and 8% higher, respectively, than those of the corresponding precured patch samples.

Therefore, according to the above-mentioned results, the curing method had a relatively small effect on the bond strength of the samples. Hence, it can be surmised that induction curing is as efficient as conventional oven curing in terms of bond strength. In addition, the test results also showed that the bond strengths were affected more by the patch fabrication method used (i.e., whether a precured or a cocured patch was used) than by the curing method used (i.e., whether oven curing or induction curing was used). These factors are discussed in detail later.

3.4.2 CNT reinforced sample

CNT reinforcements were studied to determine their effect on the strength of the DLS joint under tension loading. Five samples were tested for each CNT configuration. The bond strength data in Table 3.4 has been normalized using the maximum load value for samples with CNT reinforcement. As can be seen in Table 3.4 there is very little scatter in results for all the samples tested in tension. The maximum coefficient of variation is only 4.5% for the induction/cocured samples.

Figure 3.11 indicates that the induction-cured samples were as strong as their corresponding oven-cured samples (i.e., the induction / precured patch samples were as strong as the oven / precured patch ones). Only the fabrication method had an effect on the average strength of the samples. As with the baseline samples, each cocured patch sample pair (oven and induction curing) were about 10% and 8% stronger than their corresponding precured patch sample pair. This indicates that the curing method may have a smaller effect on the strength of the sample than the fabrication method. The addition of 0.5 wt% CNTs to the oven/precure, oven/cocure, induction/precure, and induction/cocure patch samples increased the bond strengths by 10%, 3%, 9%, and 8%, respectively, when compared to those of the corresponding baseline samples as shown in Figure 3.12. The bond strengths of the CNT-reinforced samples were higher than those of the baseline samples for the following reasons. When CNTs are inserted on both sides of the adhesive layer, the strength of the adhesive interface layer between the substrates (or the patches) is enhanced because the CNTs in the interface layer probably form

mechanically strong interlocks with the adhesive layer and the substrates (or the patches). A simple experiment was performed to verify this. Two samples were tested: one sample made of pure epoxy and the other sample made of a CNT dispersed solution used in the CNT reinforced samples discussed previously.

Comparison of the strength of the pure epoxy samples (Figure 3.13) and CNT reinforced samples (Figure 3.14) shows that the CNT reinforced samples were stronger than pure epoxy samples as shown in Figure 3.15. CNTs in the interface layer make a mechanically strong interlocking with the adhesive layer and substrates (or patches). Therefore, we performed an experiment to understand the CNT interlocking mechanism. We made the same schematic DLS samples as mentioned previously, except for adhesive film. There was pure epoxy resin and dispersed CNT resin solution between the aluminum substrate and patch. Two samples were tested in the same environment, and the results are shown in Figure 3.16. The CNT-reinforced DLS samples were stronger than the pure epoxy DLS samples because CNTs prevent slipping when subjected to shear loads.

3.4.3 Fracture surface of sample

Figure 3.17 shows the fracture surfaces of the tested samples. The images in Figure 17(a) show the aluminum-side fracture surfaces, while those in Figure 17(b) show the patch-side fracture surfaces. The oven/cocured patch samples, which were stronger than the other samples, had a small, adhesive-free empty

area on the aluminum side as well as on the patch side. On the other hand, the induction/precured patch samples, which were weaker than the other samples, had a large, adhesive-free area on both the aluminum side and the patch side. This means that the adhesion between the cocured patches and the aluminum substrates was stronger. This is likely because an even compressive load may have been applied during curing, owing to the lower stiffness of the uncured prepregs. Hence, the failure of the cocured samples was more likely to occur in the adhesive layer than at the interface failure.

3.4.4 Effect of cocuring procedures

3.4.4.1 Bondline profile

Surface roughness has a significant effect on the bond strength of adhesive bonds [2]. Mechanical interlocking between the adhesive and the substrate contributes significantly to the durability of joints. These facts suggested that the bondline profile may introduce an interfacial shear component at the adhesive-to-substrate interface and that this shear component might improve the fracture toughness of the joints. The bondline profile is critical to achieving durable adhesive bonds. An undulated profile leads to higher bond strength. Therefore, we determined the bondline profiles of the samples along the interface between the adhesive and the patch.

3.4.4.2 Bondline profile analysis

Optical microscopy-based analyses of the samples were performed to obtain information regarding the bondline profiles. The bondline profiles of the oven/precure, oven/cocure, induction/precure, and induction/cocure baseline samples are shown in Figure 3.18, Figure 3.19. It should be noted that the bondline profiles of the precured and cocured samples were significantly different. The precured patch samples (oven/precure as well as induction/precure) had a relatively straight bondline profile, in contrast to those of cocured patch samples (oven/cocure as well as induction/cocure). The bondline profiles of the CNT-reinforced samples were similar to those of the corresponding baseline samples.

We quantitatively measured the bondline profiles of the samples using optical microscopy. Five places of same interval were measured along 1.5mm length. The standard deviation values of the bondline profiles of samples are shown in Table 3.5 and Figure 3.20. The standard deviation values of the bondline profiles for all the precured patch samples were 1.2–3.5 μm, while the standard deviation values of the cocured patch samples were approximately 6.3–11.9 μm. In other words, the cocured patch samples had a more undulated bondline profile than did the precured patch samples; this was true for both the baseline and the CNT-reinforced samples. As was noticed previously, the cocured patch samples exhibited higher bond strengths than those of the corresponding

precured patch samples; again, this was true for both the baseline as well as the CNT-reinforced samples.

3.4.4.3 Deliberately patterned patch

We performed another experiment to validate the bondline profile effect. A precured patch was made with a patterned stamp inserted into a hot press, as shown in Figure 3.21. A fabric peel ply was placed above the patterned stamp and eight plies of unidirectional prepreg were cured by the hot press. The cure cycle was 90 minutes at 120 °C. The comparison of the patch roughness is shown in Figure 3.22. The non-treated patch, 220-sandpaper treated patch, and deliberately patterned patch had about 0.2 μm, 0.8 μm, and 12 μm of roughness, respectively, as shown in Figure 3.23. The roughness of the deliberately patterned patch had a larger roughness than the other samples. Sample fabrication was identical to that mentioned previously and the bond strength was tested. Figure 3.24 shows the comparison of test results for each case. The sample made by a deliberately patterned patch did not show a dramatic bond strength improvement.

3.4.4.4 FT-IR analysis of bondline interface

FT-IR (Fourier Transform InfraRed) offers several advantages. First, it allows one to monitor the curing process over the whole conversion range. In

fact, although during curing the material undergoes several state transitions from fluid to rubbery to glass, these transitions have limited influence on the vibration spectrum. Second, by selecting the appropriate signals, it is possible to monitor simultaneously the concentration profiles of the various reacting species present in the system, which is the only way to obtain direct mechanistic information. A third important consideration arises when working in the near-infrared (NIR) range, which extends between 10,000 and 4000 cm^{-1}. This radiation travels very efficiently through commercially available optical fibers, thus allowing an *in situ* remote monitoring of the process [36].

We conducted FT-IR (Fourier Transform InfraRed) spectroscopy analysis for the cured adhesive film, cured carbon fiber epoxy prepreg patch, and the interface of each bonding surface. The purpose of the FT-IR spectrum analysis is to look for whether cocuring creates other chemical bonding at the interface of the adhesive film and cocured prepreg patch. The composition of the adhesive film and carbon epoxy prepreg are epoxy resin based. The FT-IR spectrum of cured the adhesive film and cured prepreg patch is shown in Figure 3.26. It agrees with the FT-IR spectrum of basic epoxy resin shown in Figure 3.25 [36]. Several bonding interface points were analyzed but there are no other chemical bonds present, as shown in Figures 3.27 and 3.28. Therefore, we only found a basic epoxy chemical bonding at the interface of the cured adhesive film and cured prepreg patch. This results in increased bond strength of the cocuring samples.

3.5 Fracture simulation of sample

3.5.1 Theory and model

We present a model for the double lap joint sample illustrated in Figure 3.29. When the repaired sample is subjected to a tensile load, the interlayer may fail in shear. There are four possible scenarios for the behavior of the interlayer: the entire interlayer behaves in a linearly elastic manner, there is a perfect plastic region either near the x = 0 or near the x = d_1 end of the interlayer, or there are perfect plastic regions near both the x=0 and x=d_1 ends of the interlayer (Figure 3.30) [37]. The shear strains at the elastic limit and at plastic failure are γ_{ef} and γ_{pf}, respectively.

3.5.2 Simulation process and results

We conducted a simulation to calculate the failure loads and modes of the patch repaired sample. The sample is assumed symmetric for the simulation and it is sufficient to consider only one-half of the sample, as shown in Figure 3.29. ABAQUS was used to calculate the load. The results of the simulation are shown in Figure 3.31. The interlayer failure behavior of the sample begins at x = d_1 and 0.17 s, as shown in Figure 3.31.

We compared the load-displacement results between simulation and

experiment. The results shown in Figure 3.32 indicate that the simulation results are similar to the experimental results.

3.6 Advantages of induction heating

3.6.1 Simulation of temperature rise rate

We conducted a simulation to compare the temperature rise rate of the adhesive area between the induction heating and heat blanket. The heat blanket was considered an oven, which was used in the previous section. When the temperature rises up to 120 °C for 20 minutes, we checked the temperature change of the adhesive area. The final temperature distributions are shown in Figure 3.33 after 20 minutes. Heat from the adhesive film was conducted from the aluminum during induction heating curing, but the heat from the adhesive film using the heat blanket curing was convected through the patch.

3.6.2 Results of simulation

The results of the simulation to compare the temperature rise rate of the adhesive area between induction heating and heat blanket are shown in Figure 3.34. The black line/cross point is the input temperature of induction and heat blanket, respectively. The red line/bar point and blue line/triangle point are the temperature rise rate of the adhesive area for induction heating and the heat

blanket, respectively. The temperature rise rate by induction heating corresponded with the input temperature, but the temperature rise rate by the heat blanket lagged the input temperature by 200 s. This shows that induction heating is a faster and more efficient method than the heat blanket for curing adhesive of a composite patch. The induction heating techniques allows rapid heating of the adhesive material and through thermal conduction, rapid heating of the adjacent adhesive.

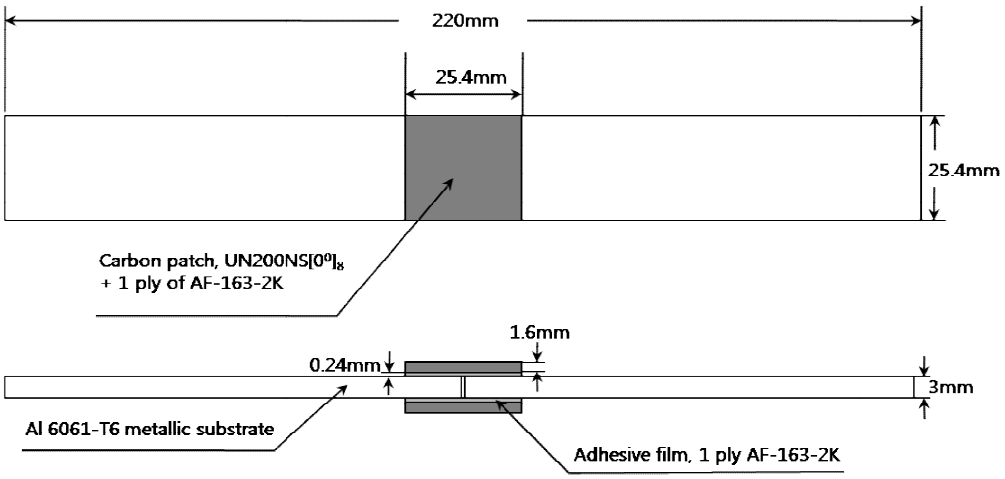

Figure 3.1 Schematic of patch sample configuration (not to scale)

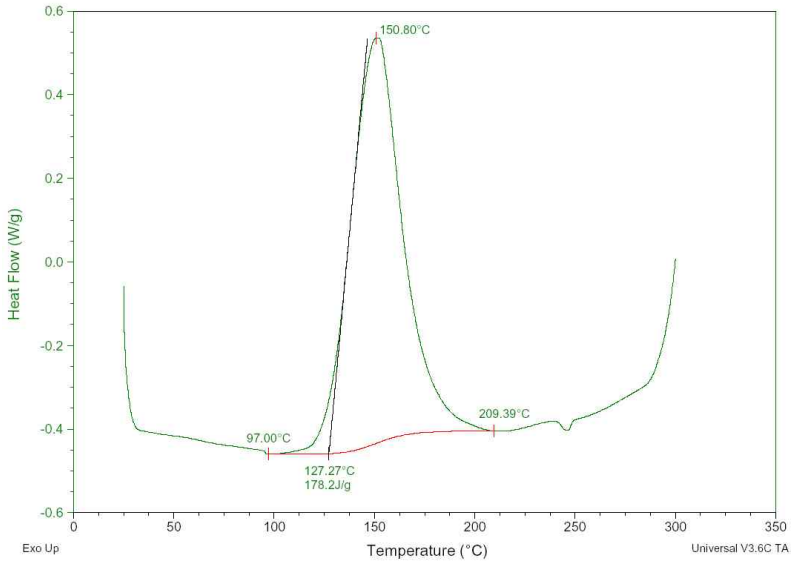

Figure 3.2 DSC heat flow of AF-163-2k film adhesive

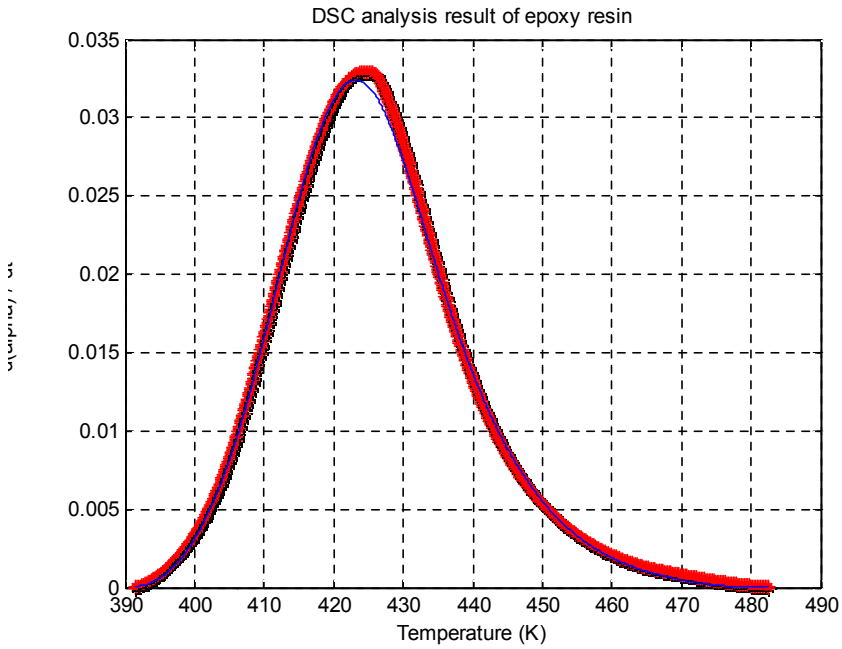

Figure 3.3 Modeling of cure kinetics by curve fitting of adhesive film (AF-163-2K)

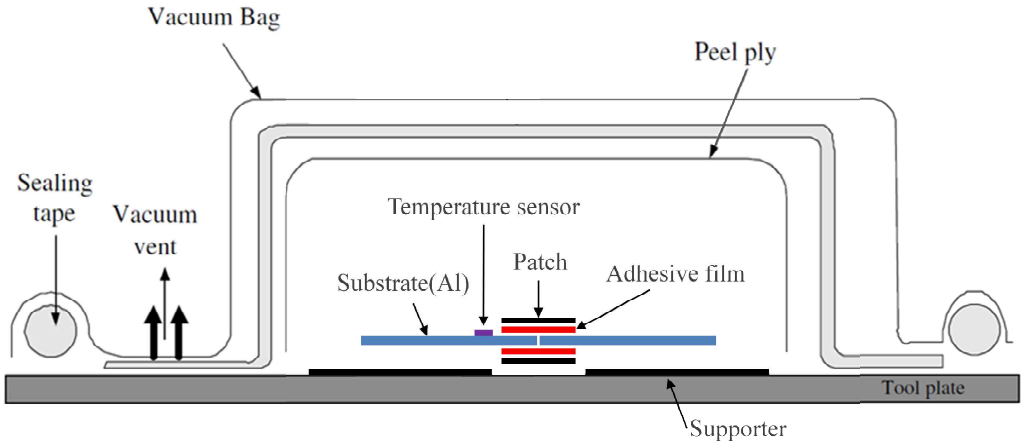

Figure 3.4 Sample preparation for oven and induction curing

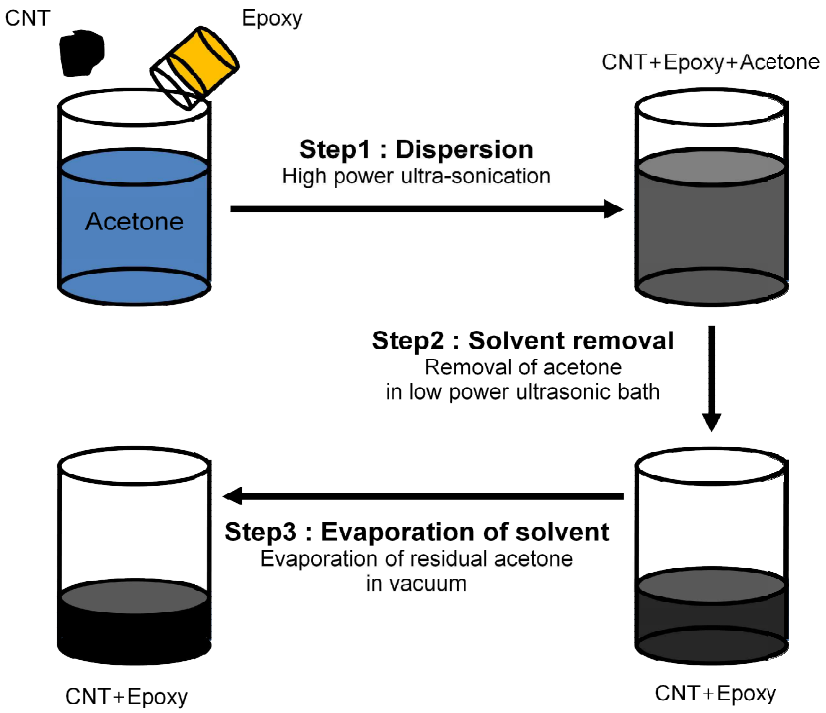

Figure 3.5 CNT dispersion process

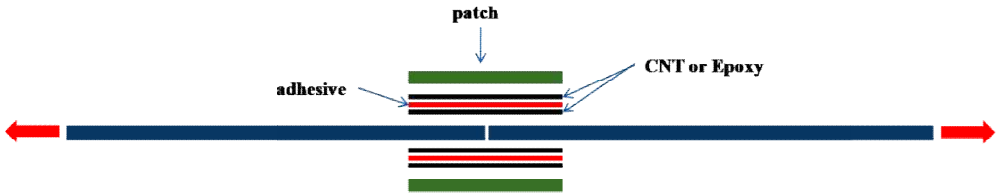

Figure 3.6 Schematic of CNT reinforced sample

Figure 3.7 Curing cycle of oven and induction

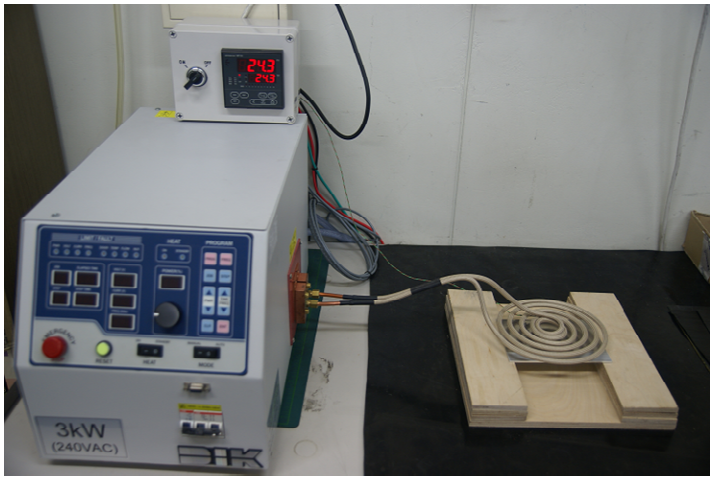

Figure 3.8 Overview of induction heater

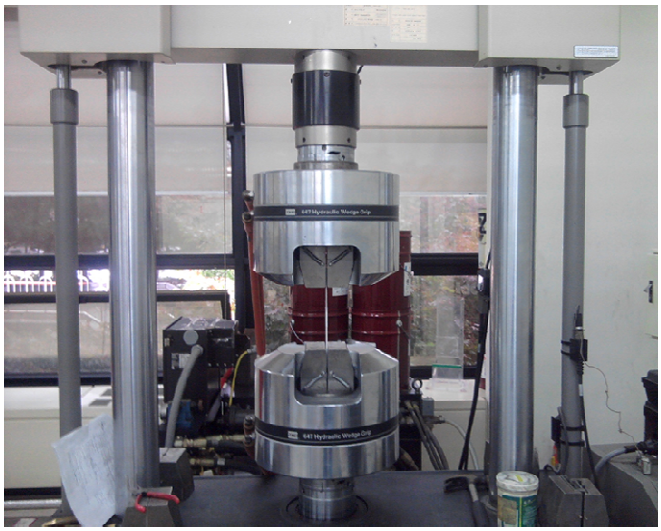

Figure 3.9 Overview of test machine(Instron 810)

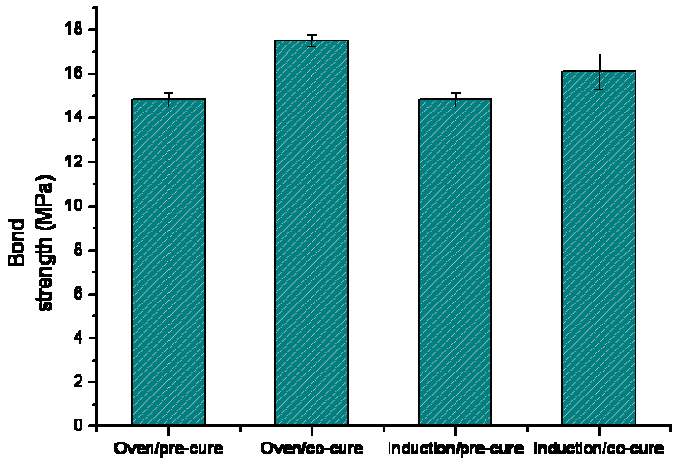

Figure 3.10 Double lap joint sample without CNT (baseline sample)

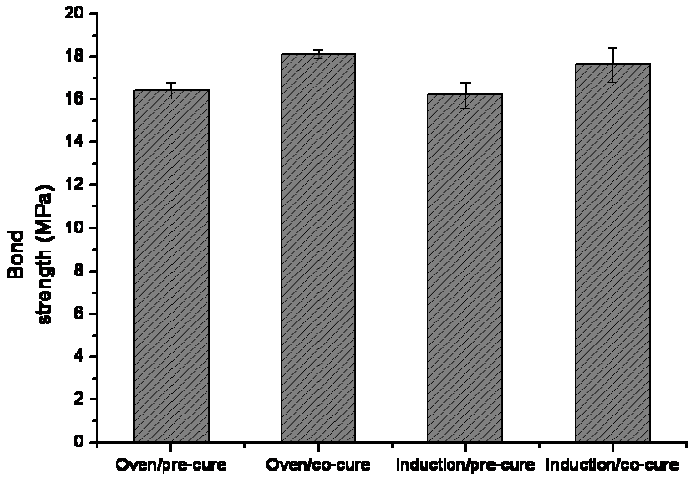

Figure 3.11 Double lap joint sample with CNT reinforcement

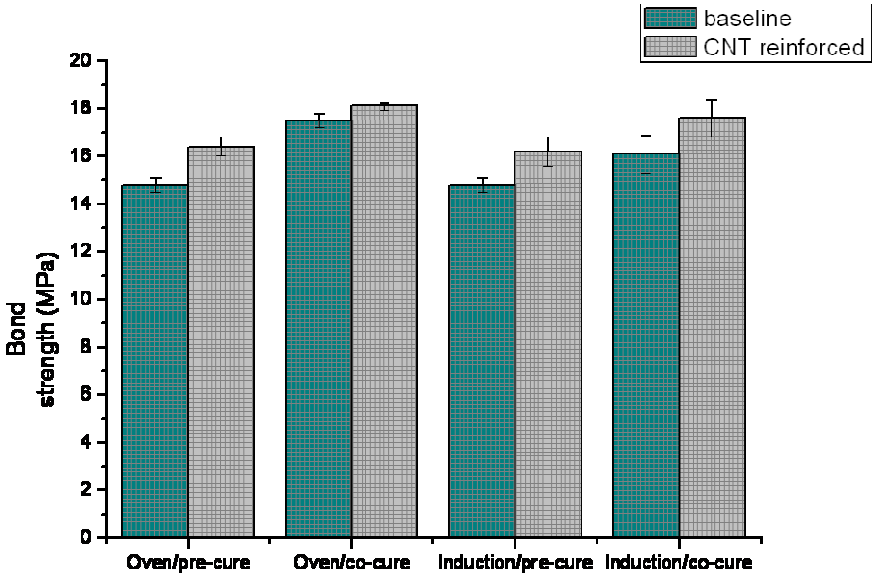

Figure 3.12 Comparison strength of baseline and CNT reinforced samples

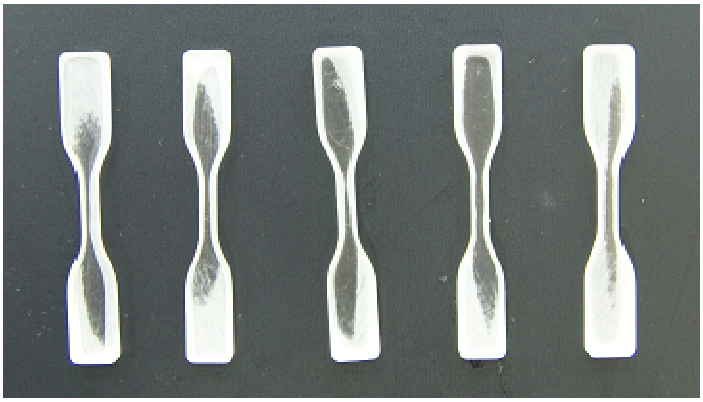

Figure 3.13 Epoxy resin samples

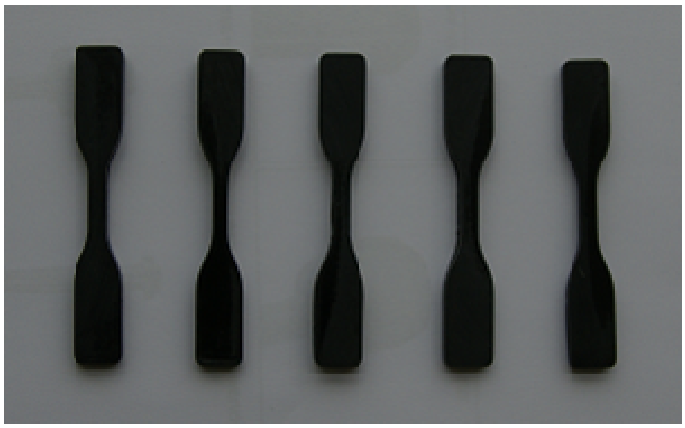

Figure 3.14 CNT reinforced resin samples

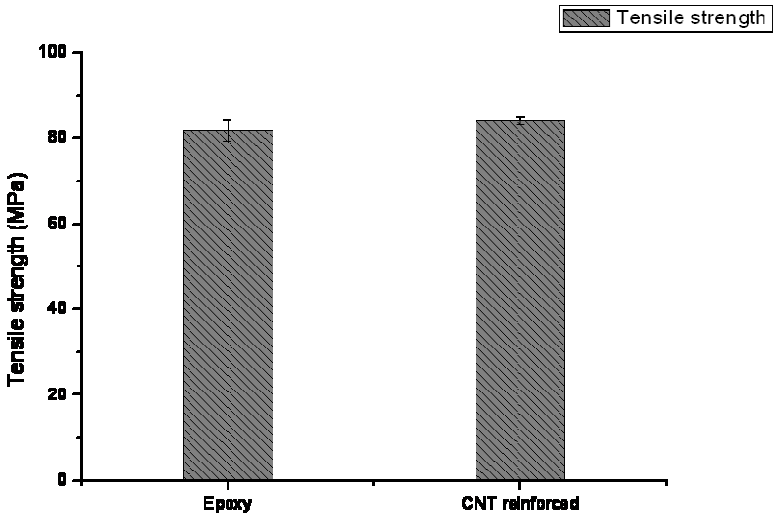

Figure 3.15 Strength comparison between epoxy and CNT samples

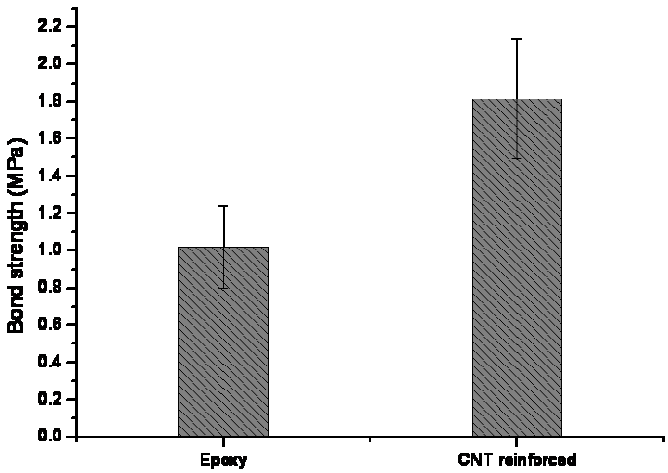

Figure 3.16 Strength comparison between epoxy and CNT DLS samples without adhesive

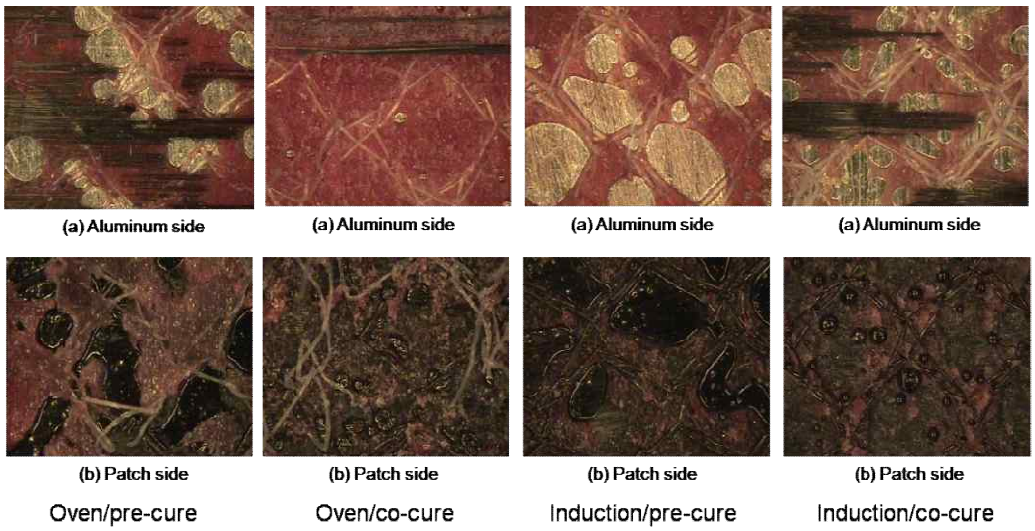

Figure 3.17 Fracture surfaces of baseline samples

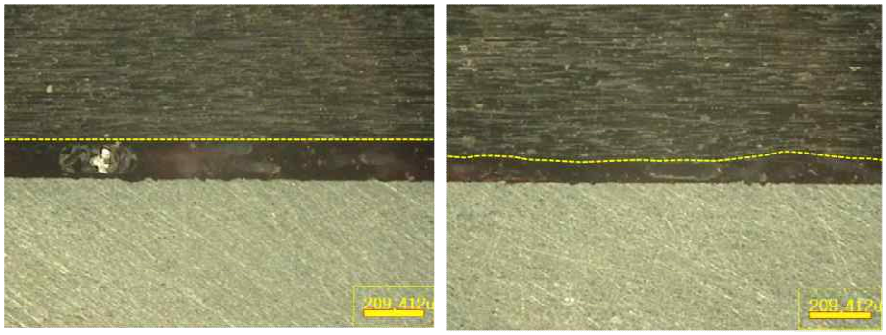

(a)Oven/precure **(b)Oven/cocure**

Figure 3.18 Bondline profile of baseline sample (x 200)

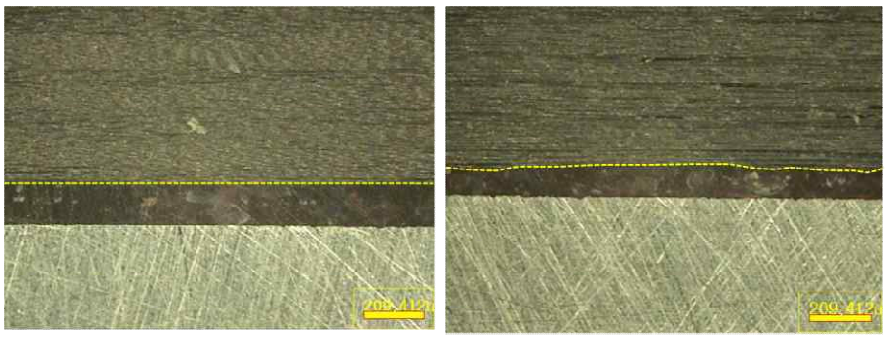

(a)Oven/precure **(b)Oven/cocure**

Figure 3.19 Bondline profile of CNT sample (x 200)

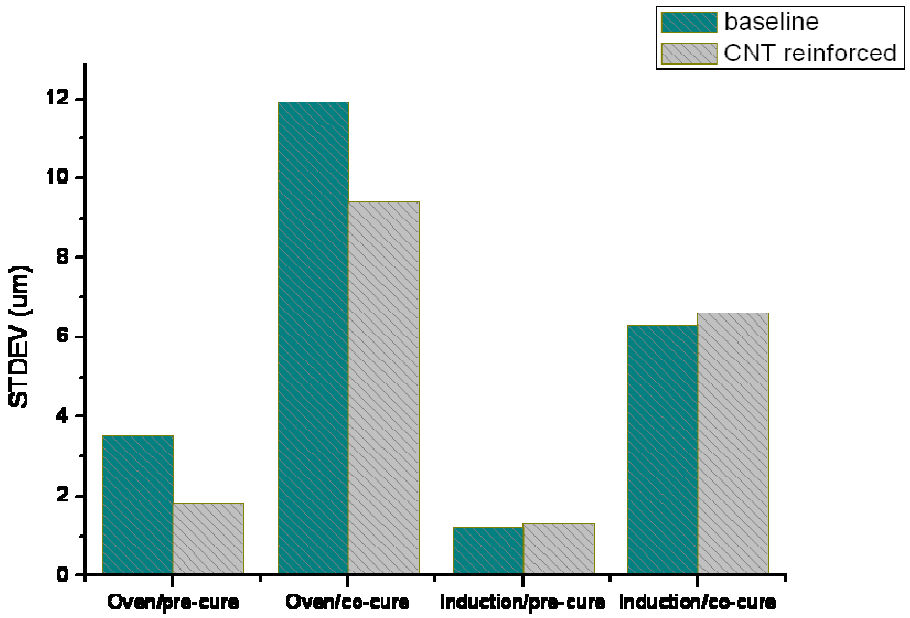

Figure 3.20 Standard deviation of bondline profile

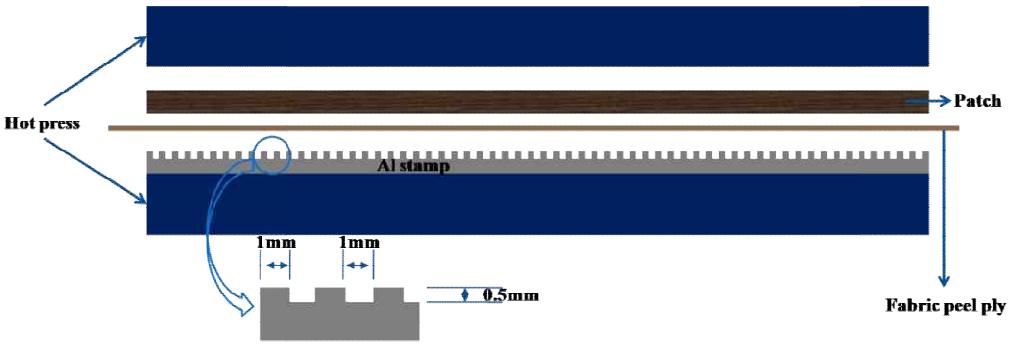

Figure 3.21 Deliberate pattern manufacturing schematic of precured patch

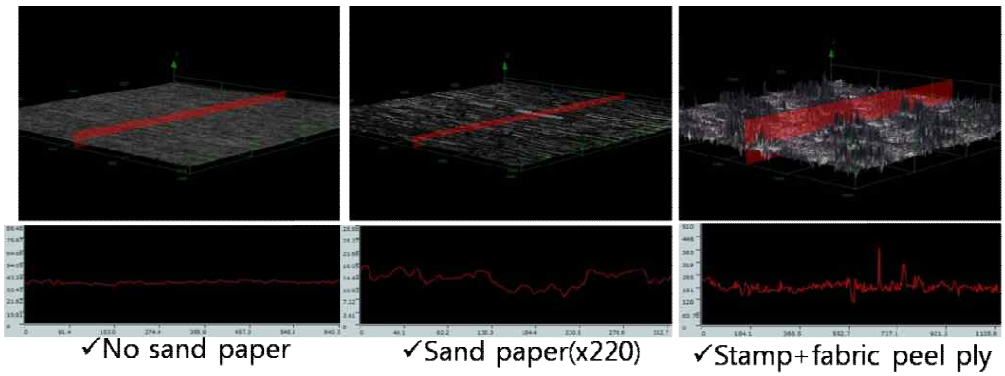

Figure 3.22 Comparison of roughness profile

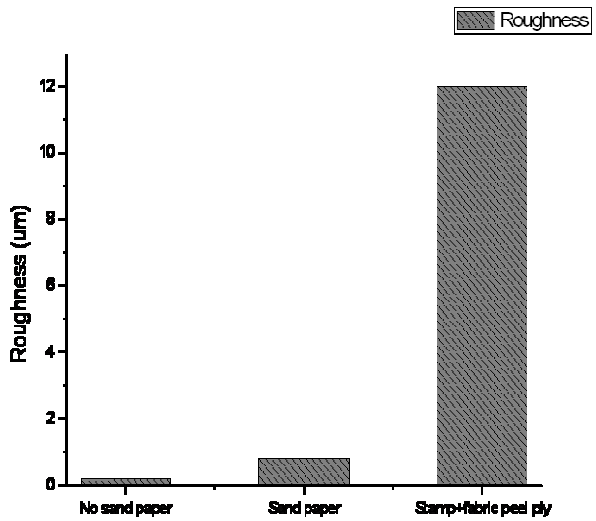

Figure 3.23 Results of roughness values

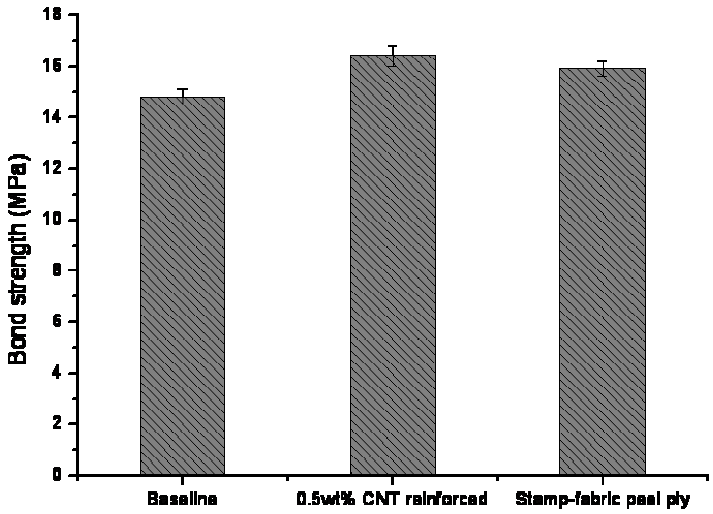

Figure 3.24 Bond strength comparison of test results

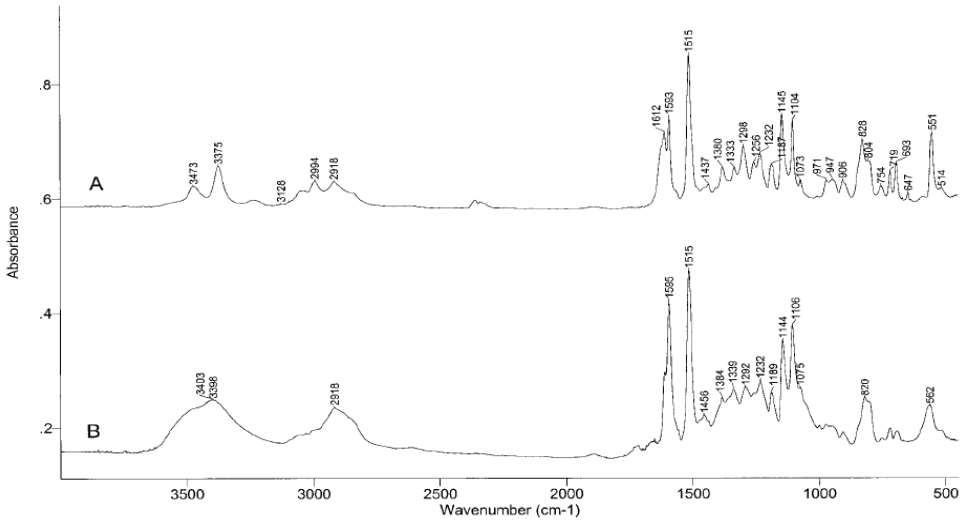

Figure 3.25 FTIR transmission spectra in the 4000–450 cm wavenumber range

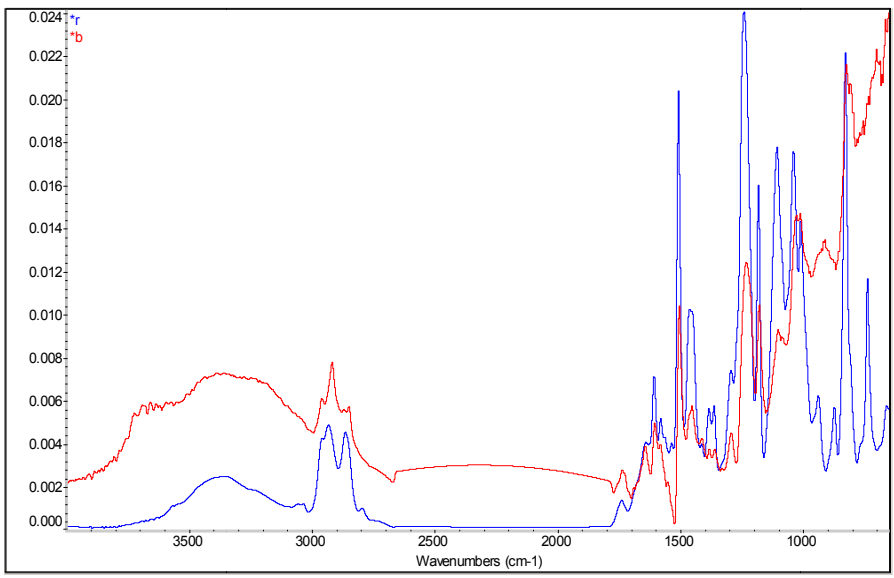

Figure 3.26 FT-IR of adhesive and patch (r: Adhesive, b: Carbon fiber patch)

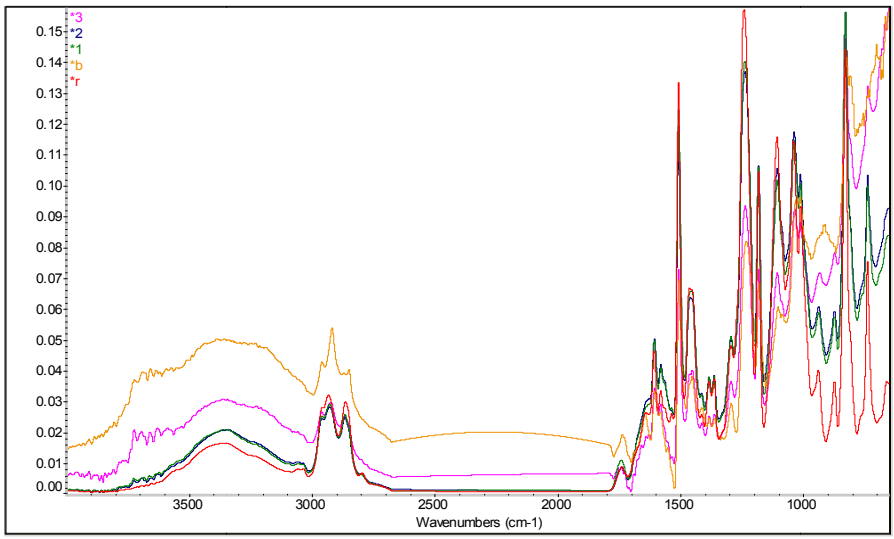

Figure 3.27 FT-IR of adhesive and patch (r: Adhesive, b: Carbon fiber patch, 1/2/3: Interface)

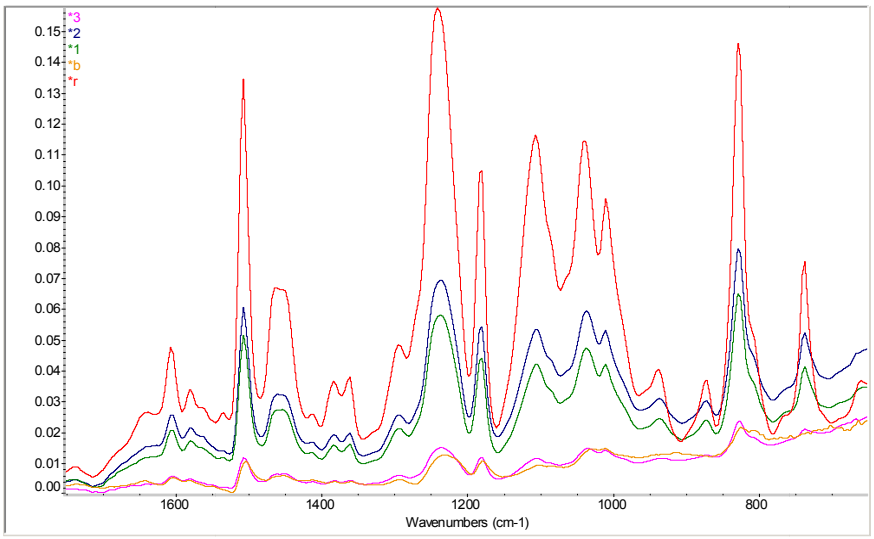

Figure 3.28 FT-IR of adhesive and patch (1700~700wavenumvers)

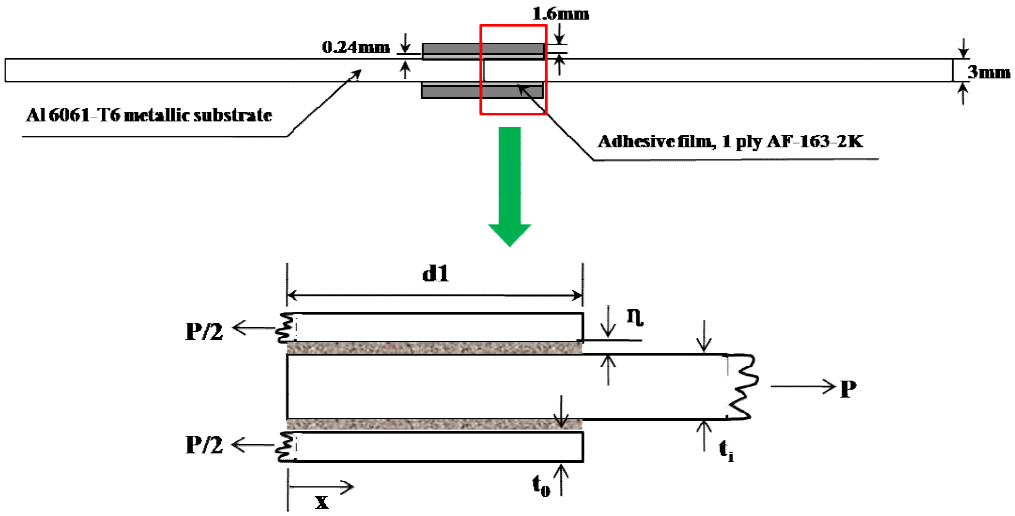

Figure 3.29 Symmetry model for fracture simulation

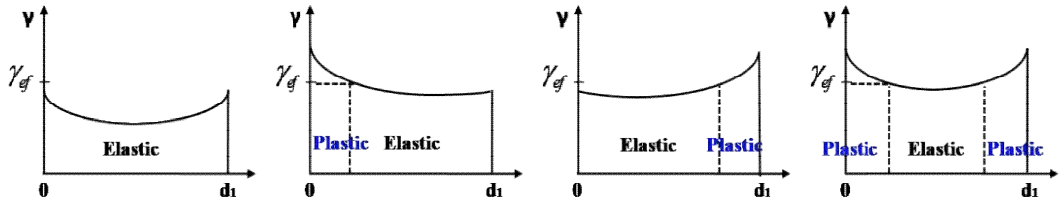

Figure 3.30 Four possible scenarios of interlayer failure

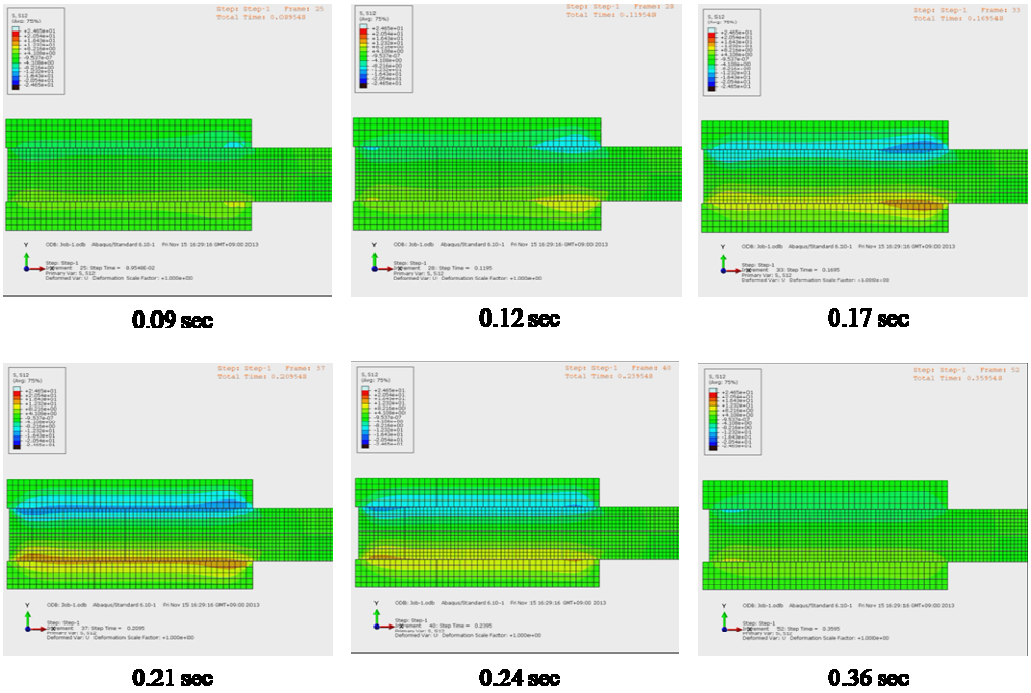

Figure 3.31 Fracture progress of sample

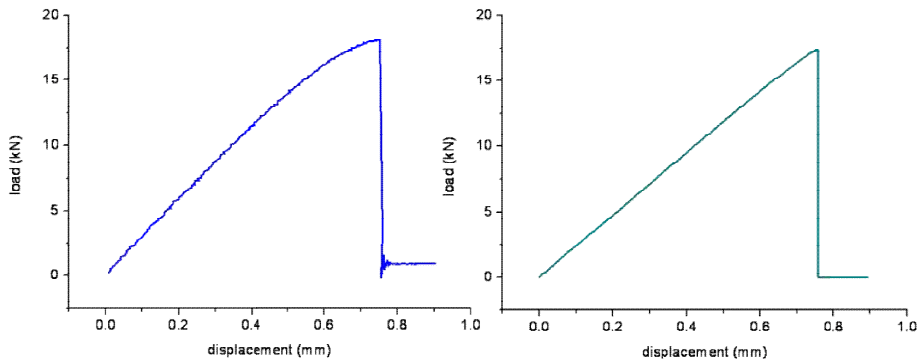

(a) Experiment **(b) Simulation**

Figure 3.32 Comparison of experiment and simulation

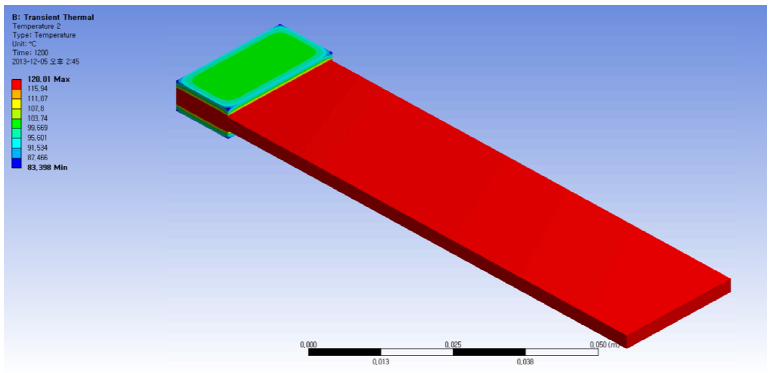

✓**Induction heating**

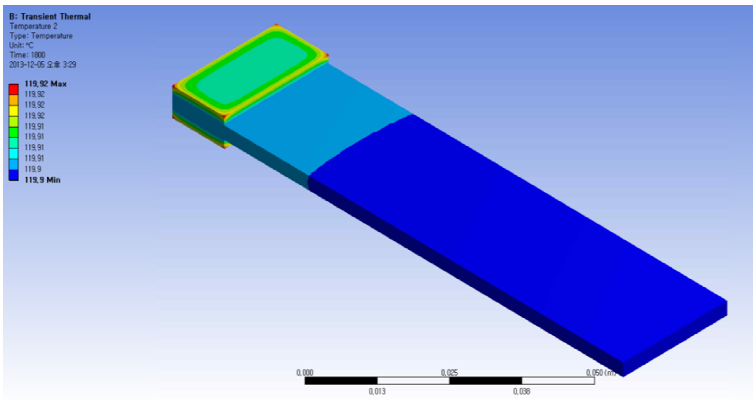

✓**Heat blanket**

Figure 3.33 Final temperature distributions of induction and heat blanket when temperature rise up to 120 ºC for 20 minutes

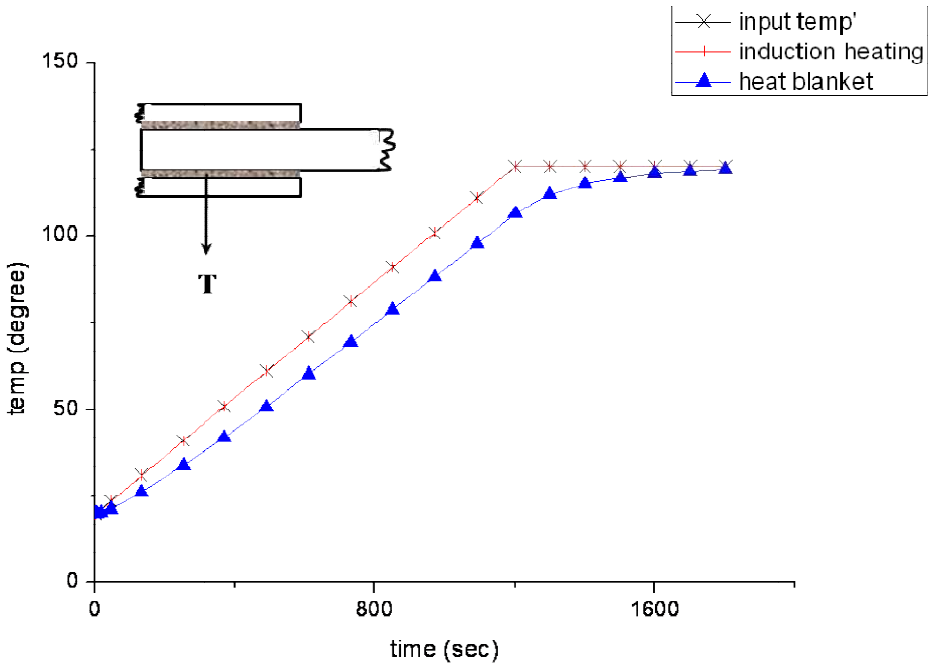

Figure 3.34 The results of simulation to compare temperature rise rate of adhesive area between induction heating and heat blanket

Table 3.1 Material properties

- Al Substrates : 6061-T6

$E_{[Gpa]}$	$G_{[Gpa]}$	ν	$\sigma_{s[Mpa]}$	$\sigma_{u[Mpa]}$
68.00	26.20	0.33	276	310

- Adhesive Film : 3M AF 163-2K

$E_{[Gpa]}$	$G_{[Gpa]}$	ν	$t_{[mm]}$
1.10	0.41	0.34	0.24

- Prepreg : Hankook carbon UN200NS

$E_{1[Gpa]}$	$E_{2[Gpa]}$	$G_{12[Gpa]}$	$G_{23[Gpa]}$	ν_{12}	$t_{[mm]}$
124	13	4.8	4.82	0.28	0.2

Table 3.2 Parameter values of adhesive film

Parameter	A_1	A_2	E_1	E_2	m	n
Value	4.14e-6	0.1102	1.0003	1.0002	0.78791	0.99603

Table 3.3 Double lap joint sample without CNT, tested in tension

	Patch	Apparent Shear Strength (MPa) [Standard Deviation]	CV (%)
Oven-cured samples	Precure	14.8[0.3]	2.0
	Cocure	17.5[0.3]	1.7
Induction-cured samples	Precure	14.8[0.3]	2.0
	Cocure	16.1[0.8]	4.9

Table 3.4 Double lap joint sample with CNT, tested in tension

	Patch	Apparent Shear Strength (MPa) [Standard Deviation]	CV (%)
Oven-cured samples	Precure	16.4[0.4]	2.4
	Cocure	18.1[0.2]	1.1
Induction-cured samples	Precure	16.2[0.6]	3.7
	Cocure	17.6[0.8]	4.5

Table 3.5 Standard deviation value of bondline profile Unit :㎛

	Oven/ precure	Oven/ cocure	Induction/ precure	Induction/ cocure
Baseline	3.5	11.9	1.2	6.3
CNT	1.8	6.9	1.3	6.6

Chapter 4

NUMERICAL ANALYSIS OF INDUCTION HEATING

Chapter 4
Numerical analysis of induction heating

4.1 Overview

We performed the experiment and numerical simulation to determine whether induction curing is an efficient technique (and whether induction heating a suitable heating method) for metallic substrates associated with the repair with aircraft. The experiments and simulations were performed to check whether the patches on aluminum substrates affected the temperature increase rate of the substrates during curing by induction heating. Three different experiments were performed under the same induction output conditions (i.e., current of 70A and frequency of 150 kHz) and numerical simulation were performed by commercial simulation program code ANSYS®. And we had compared the results between experiment and simulation.

4.2 Experiment of induction heating

4.2.1 Effect of patch for induction heating

Three different experiments were performed under the same induction output conditions (i.e., current of 70A and frequency of 150 kHz). The first experiment involved heating only an aluminum substrate by induction. The second involved heating the cured composite patch on an aluminum substrate. Finally, the third involved heating the uncured composite patch (uncured prepreg) on an aluminum substrate. Each sample was heated by induction until the temperature reached 120 °C. The experiment setup is shown in Figure 4.1. The distance between the aluminum substrate and the induction coil was 11 mm. We determined the rate of temperature increase of the aluminum substrate using a thermistor-based temperature sensor placed between the aluminum substrate and the patches.

4.2.2 Results of experiment

The efficiency of inducting heating is dependent on the electrical and thermal conductivities of the materials placed between the aluminum substrate and the induction heating coil. As shown in Figure 4.2, the temperature of the aluminum substrate increased at a greater rate when only the substrate was heated than when the aluminum substrate was heated while having an uncured

patch placed on top of it. It took 30 min to heat the aluminum substrate to 120 °C in the former case, while the temperature reached only 116 °C after 80 min in the latter case. This is presumably because the heat generated by induction heating is transferred to the uncured patch, resulting in the curing of the prepreg. Meanwhile, the assembly consisting of a cured patch placed on top of the aluminum substrate heated more quickly than did the aluminum substrate alone. In this case, it took only 22 min for the temperature of the assembly to reach 120 °C. This result may be attributed to the fact that the cured patch kept the aluminum substrate warm, while the aluminum substrate, when heated without a cured patch, was exposed to the environment and radiated heat. However, in real-life applications, the uncured patch would not cover the aluminum substrate completely. In other words, part of the aluminum substrate would still be exposed directly to the induction heating coil, and its temperature could increase. This was also proven by the fact that we did not experience any difficulty in processing the DLS samples with the uncured patches using induction heating.

4.3 Numerical analysis

4.3.1 Modeling method for induction heating

4.3.1.1 Theoretical backgrounds

Although the usage of multilayer induction heating systems began later than the use of conventional single layer induction heating system by many decades, however it could be noted that the methods used to analyze the induction heating. problem are, almost, the same for single or multi layer coil, where it could be considered in analytical point of view that single layer is the special case of the general (multilayer) case. The Finite Element Method (FEM) could be considered to be the fastest growing technique in the area of electromagnetic applications where many FEM-based professional packages are available to simulate various induction heating systems [38].

4.3.1.2 Mathematical modeling of the electromagnetic field

The technique of calculating electromagnetic field depends on the ability to solve Maxwell's equations. For general time-varying electromagnetic fields, Maxwell's equations in differential form can be written as [39]

$$\nabla \times \mathrm{H} = J + \frac{\partial D}{\partial t} \tag{4-1}$$

$$\nabla \times E = -\frac{\partial B}{\partial t} \tag{4-2}$$

$$\nabla \bullet B = 0 \tag{4-3}$$

$$\nabla \bullet D = \rho^{charge} \tag{4-4}$$

Where E is the electric field intensity, D is the electric flux density, H is the magnetic field intensity, B is the magnetic flux density, J is conduction current density, and ρ^{charge} is electric volume charge density.

More equations are required because the number of equations is less than the number of unknowns. These equations are the following relations between the field quantities:

$$D = \varepsilon E \tag{4-5}$$

$$B = \mu H \tag{4-6}$$

$$J = \sigma E \tag{4-7}$$

Where the parameters ε, μ, and σ denote, respectively, permittivity, magnetic permeability, and electrical conductivity of the material. For the most particular applications of the induction heating of metals, where the frequency of currents is less than 10MHz, the induced conduction current density J is much greater than the displacement current density ∂D/ ∂t, so the equation (4-1) can be rewritten as:

$$\frac{d\alpha}{dt} = (k_1 + k_2\alpha^m)(\alpha_u - \alpha)^n \tag{4-8}$$

The magnetic flux density can be expressed in terms of magnetic vector potential A as:

$$B = \nabla \times A \tag{4-9}$$

And then from equations (4-2) and (4-9), it follows that

$$\nabla \times E = -\nabla \times \frac{\partial A}{\partial t} \tag{4-10}$$

Therefore, after integration, one can obtain:

$$E = -\frac{\partial A}{\partial t} - \nabla \varphi \tag{4-11}$$

Where φ is the electric scalar potential and equation (4-7) can be written as:

$$J = -\sigma \frac{\partial A}{\partial t} + \boldsymbol{J}_S \tag{4-12}$$

Where $\boldsymbol{J}_S = -\sigma \nabla \varphi$ is the source (excitation) current density in the induction coil. Neglecting the hysteresis, it can be shown that [40]

$$\nabla \times \frac{1}{\mu} \nabla \times A + \sigma \frac{\partial A}{\partial t} = \boldsymbol{J}_S \tag{4-13}$$

For the great majority of induction heating applications, a heat effect, due to hysteresis losses, does not typically exceed 7% compared to the heat effect due to eddy current losses. Therefore, an assumption of neglecting the hysteresis is valid [30].

Equation (4-13) can be rewritten as follows according to the regions of the induction heating system [33]:

For work-piece:

$$\nabla \times \frac{1}{\mu} \nabla \times A + \sigma \frac{\partial A}{\partial t} = 0 \tag{4-14}$$

For induction coil:

$$\nabla \times \frac{1}{\mu_0} \nabla \times A + \sigma_{ind} \frac{\partial A}{\partial t} = \boldsymbol{J}_S \tag{4-15}$$

Where σ_{ind} is the conductivity of coil material.

For air:

$$\nabla \times \nabla \times A = 0 \tag{4-16}$$

It can be shown that for the great majority of induction heating applications it is possible to further simplify the mathematical model by assuming that the currents have a steady-state quantity [30]. Thus a time-harmonic electromagnetic field can be introduced. This field can be described by the following equation [39]

$$\frac{1}{\mu} \nabla^2 A = -J_S + j\omega\sigma A \tag{4-17}$$

Equation (4-17) is valid for general three-dimensional fields and allows one to find all of the required design parameters of induction system such as current, power, coil impedance, and heat source density induced by eddy currents. For many induction heating applications, the quantities of the magnetic field may be assumed to be entirely directed. This allows one to reduce the three-dimensional field to a combination of two-dimensional forms.

4.3.1.3 Mathematical modeling of the thermal processes

In general, the transient heat transfer process in a metal work-piece can be

described by Fourier equation [41]:

$$c\rho_D \frac{\partial T}{\partial t} + \nabla \bullet (-k\nabla T) = \dddot{q} \tag{4-18}$$

Where T is the temperature, ρ_D is the density of metal, c is the specific heat, k is the thermal conductivity of the metal, and $\dddot{q}$ is the heat source density induced by eddy currents per unit time in a unit volume (so-called heat generation). This heat source density is obtained by solving the electromagnetic problem. For most engineering induction heating problems, boundary conditions combine the heat losses due to convection and radiation. In this case the boundary condition can be expressed as [41]:

$$-k\frac{\partial T}{\partial n} = h_f(T_S - T_a) + C_S(T_s^4 - T_a^4) + Q_s \tag{4-19}$$

Where $\frac{\partial T}{\partial n}$ is the temperature gradient in a direction normal to the surface at the point under consideration, h_f *is* the convection surface heat transfer coefficient, C_s is the radiation heat loss coefficient which can be determined approximately as $C_s=\sigma_{SB}\varepsilon_s$ where ε_s is the emissivity of work-piece and σ_{SB} is Stevan-Boltzmann constant, Q_s is the surface loss (during cooling phase or as a result of work-piece contact with cold rolls or water cooled guides, etc.), T_s is the surface temperature and T_a is the ambient temperature. If the heated body is geometrically symmetrical along the axis of symmetry, the Neumann boundary condition can be formulated as [42]:

$$\frac{\partial T}{\partial n} = 0 \tag{4-20}$$

The Neumann boundary condition implies that the temperature gradient in a direction normal to the axis of symmetry is zero.

In the case of heating a cylindrical work-piece, equation (4-19) can be rewritten as [33]:

$$c\rho_D \frac{\partial T}{\partial t} = \frac{\partial T}{\partial Z}\left(k\frac{\partial T}{\partial Z}\right) + \frac{1}{R}\frac{\partial}{\partial R}\left(kR\frac{\partial T}{\partial R}\right) + q \tag{4-21}$$

Equation (4-21) with boundary conditions (equations (4-19) and (4-20)) are the most popular equations for mathematical modeling of the heat transfer processes in induction heating and heat treatment applications.

4.3.2 Simulation process

Numerical simulations were performed to elucidate further the effects of the composite patches on the temperature increase rate during induction heating. The simulations were performed using the commercial simulation software ANSYS®. The numerical model was designed to imitate the experimental setup. The induction coil was placed 11 mm above the aluminum plate. We simplified the model to a two-dimensional axi-symmetric one to reduce the simulation time. The material properties used for the simulation are listed in Table 4.1.

The parameters considered during the simulations were the initial current density in the coil, the heating time, and the frequency of the current. The

induction output conditions employed in the simulation were the same as those used in the experiments: a coil current of 70 A at a frequency of 150 kHz and an application of 30 min. The numerical simulation process, including the governing equations used for the analysis, is shown in Figure 4.3. As mentioned previously, the analysis domain was simplified by using a two-dimensional axi-symmetric model in which the heating section was considered to be rotationally symmetric. Figure 4.4 shows the two-dimensional axi-symmetric model used. Simulations involving an aluminum substrate alone and those involving an aluminum substrate with a procured and uncured patch on top of it and heated using an induction were performed under similar conditions. The temperature increase rate was determined for a heating period of 30 min in each case. The magnetic field intensity and temperature are related to the magnetic permeability while the temperature is also related to the specific heat, thermal conductivity, and electrical resistivity.

4.3.3 Results of simulation

4.3.3.1 Only aluminum substrates model

Figure 4.5 shows the distribution of the magnetic flux and magnetic density in the heating section in the case of the aluminum substrate without a patch. In this case, the magnetic field is concentrated around the inter coil. The Figure 4.6

shows the temperature and heat flux distribution in the case of the aluminum substrate without a patch. At the end of the heating stage (i.e., at 25 min), the temperature of the surface aluminum substrate was 120 °C.

4.3.3.2 Precured patch on aluminum substrates model

Figure 4.7 shows the 2-D axi-symmetric model of patched (precured & uncured patch) aluminum substrates. Figure 4.8 shows the distribution of the magnetic flux and magnetic density in the heating section in case of the assembly consisting of a precured patch on an aluminum substrate. Figure 4.9 shows the temperature distribution and heat flux in case of this assembly. At the end of the heating stage (i.e., at 30 min), the temperature of the surface of the aluminum substrate was 152 °C.

4.3.3.3 Uncured patch on aluminum substrates model

Figure 4.10 illustrates the distribution of the magnetic flux and density in the heating section. Figure 4.11 shows the temperature distribution and heat flux. Like the precured patch model, at the end of the heating stage (30 min), the maximum temperature is 109 °C on the surface of the aluminum substrates.

4.4 Results and discussion

The results of the simulations confirmed that the effect of composite patches on the induction heating of aluminum substrates was minimal and that they did not restrict the magnetic flux from passing through them. In addition, the aluminum substrates with a precured patch exhibited a higher temperature increase rate since the patch kept the aluminum substrates warm, as was seen during the experiments as well. Meanwhile in uncured patch assembly, the generated heat by induction heating was transferred to the uncured patch. So uncured patch assembly has a slow heat-up rate than only aluminum substrates. A comparison of the experimental results and the simulation results is shown in Figure 4.12. The simulation results were almost similar to the experimental results. The cause of the differences is the error in the simulation of induction heating, because only the effects of eddy currents were taken into consideration during the simulation, while those of hysteresis loss were ignored. This was because eddy currents form the basis of induction heating.

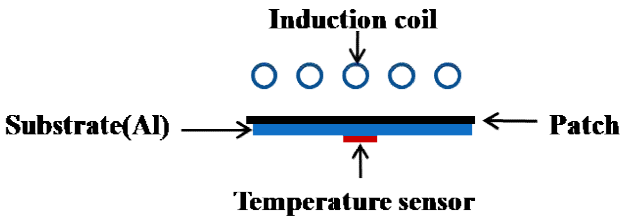

Figure 4.1 Experiment set up

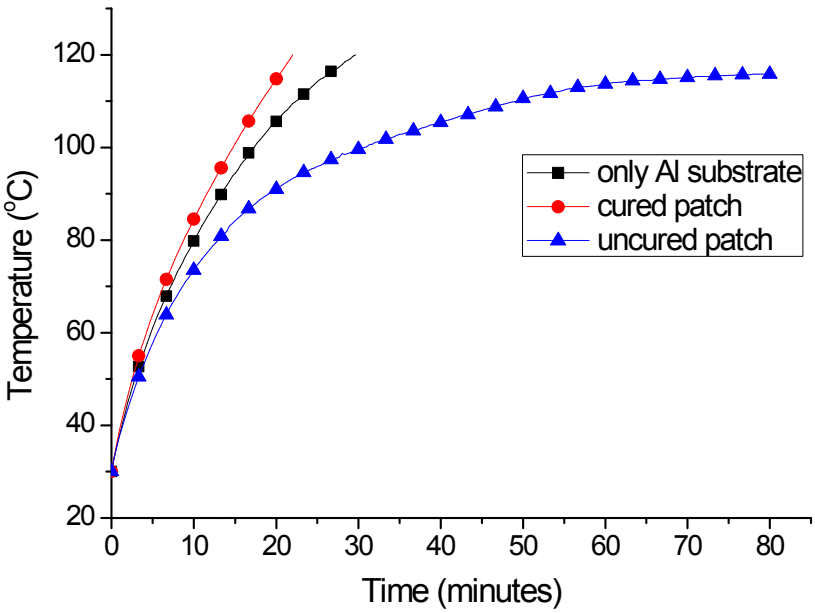

Figure 4.2 Experiment results of patch effect for induction heating

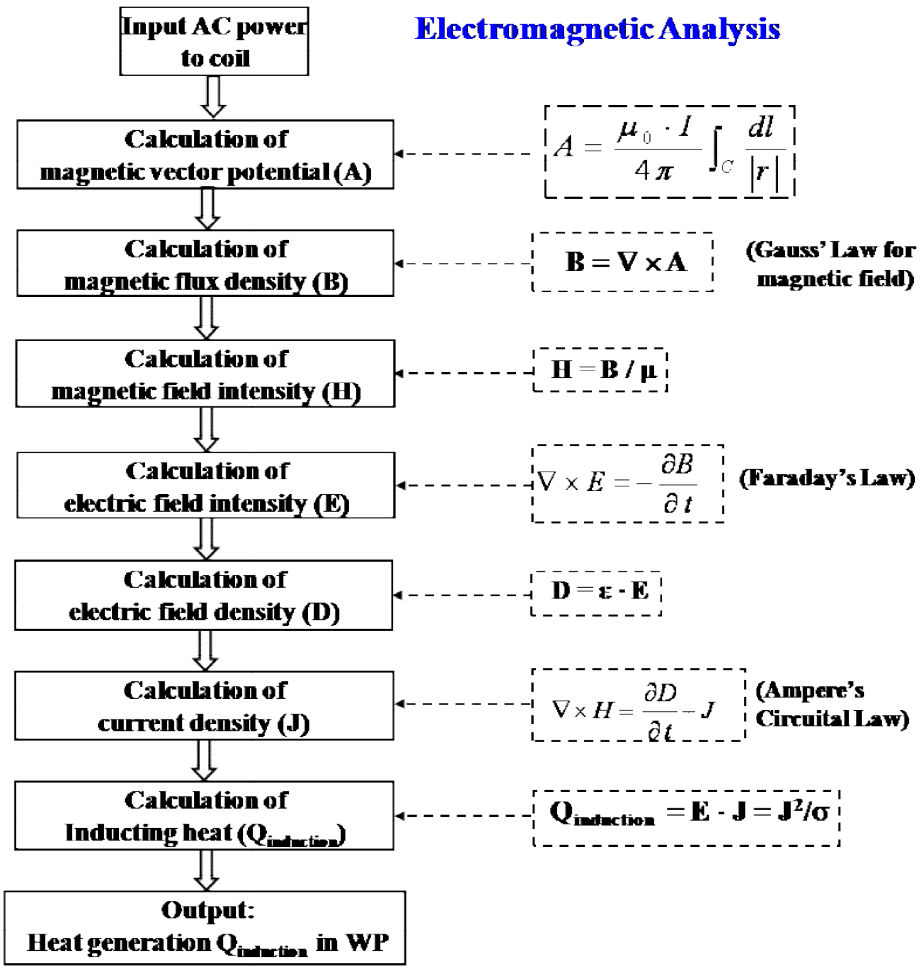

Figure 4.3 Governing equations of numerical simulation process

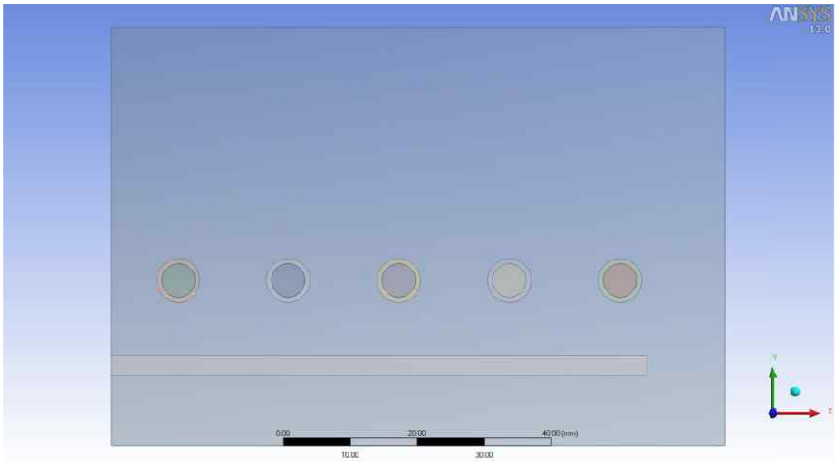

Figure 4.4 2D model for induction heating

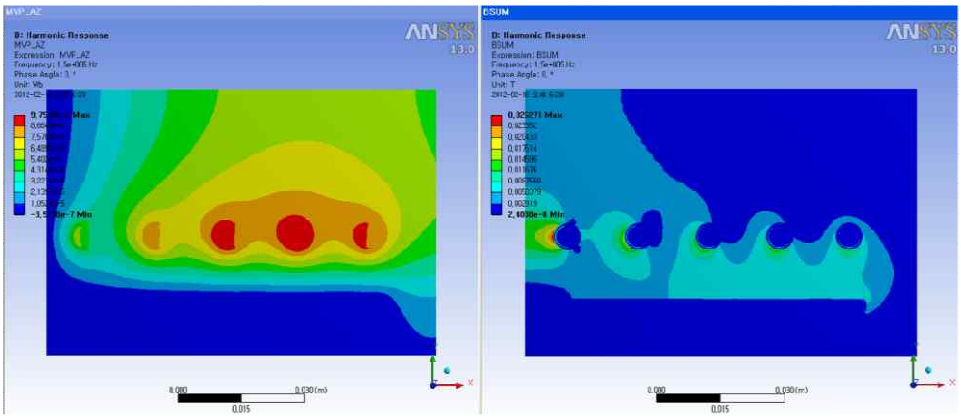

Figure 4.5 Magnetic flux and density of only Al substrate

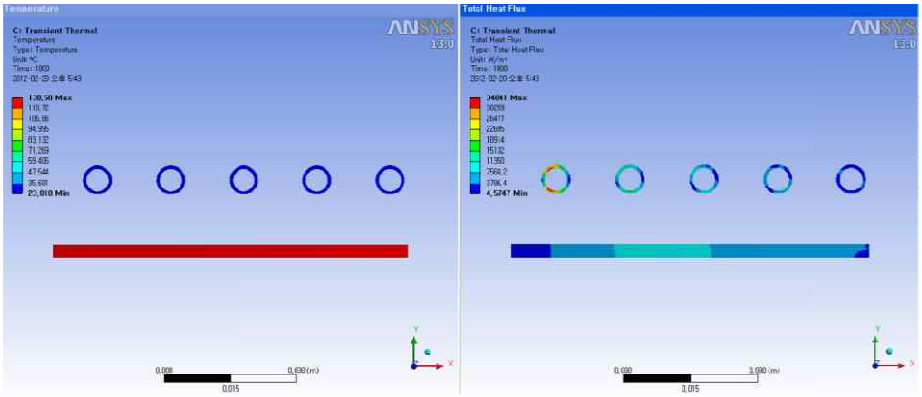

Figure 4.6 Temperature and heat flux of only Al substrate

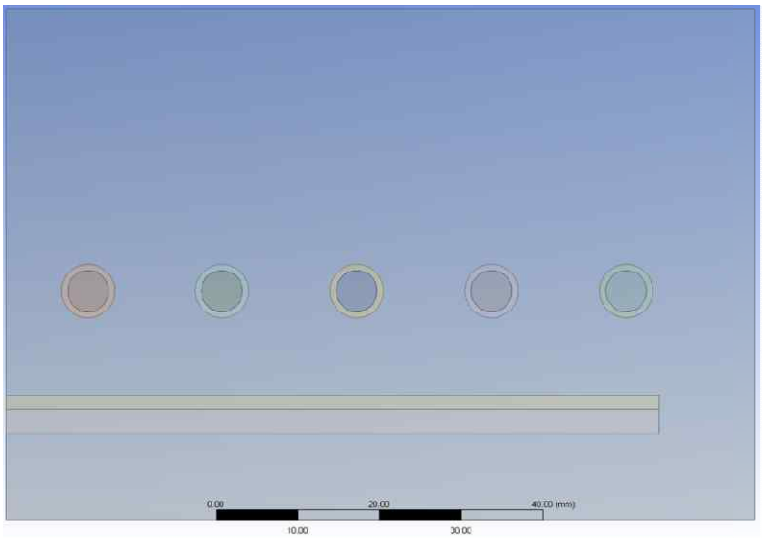

Figure 4.7 2D model with patch for induction heating

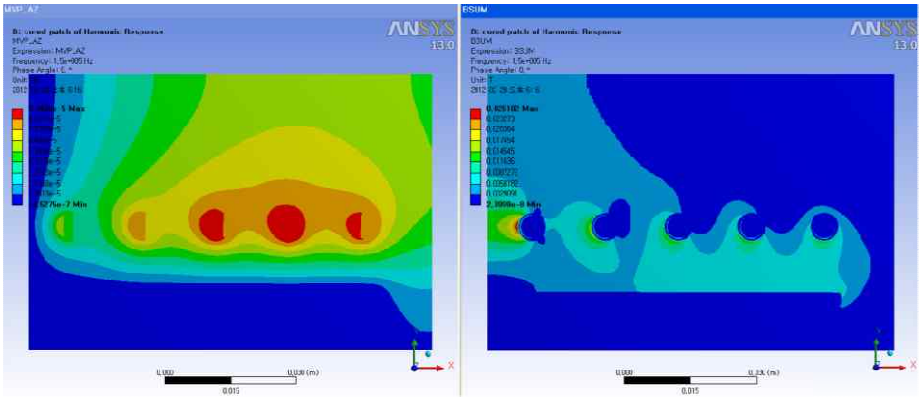

Figure 4.8 Magnetic flux and density of precured patch on Al substrate

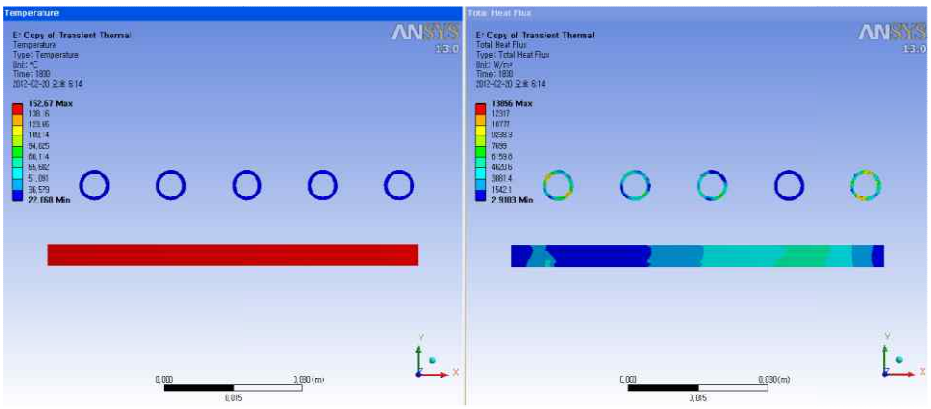

Figure 4.9 Temperature and heat flux of precured patch on Al substrate

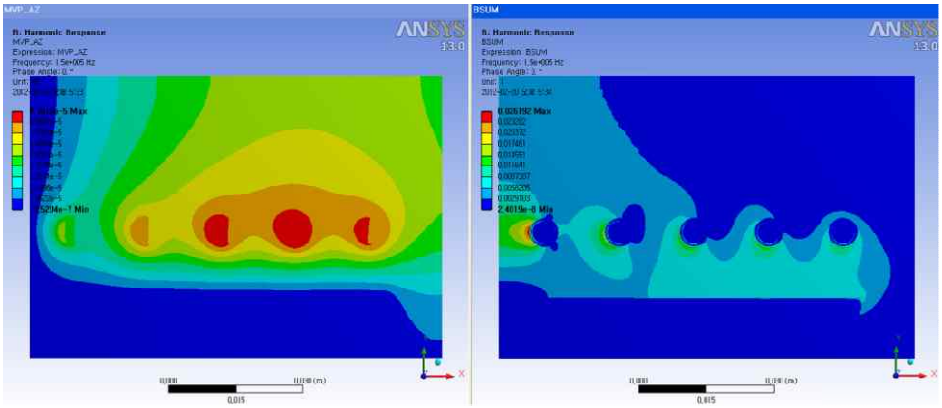

Figure 4.10 Magnetic flux and density of uncured patch on Al substrate

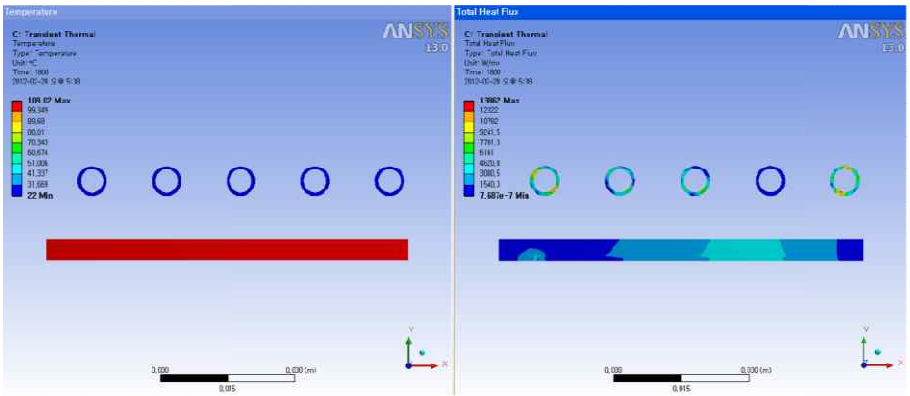

Figure 4.11 Temperature and heat flux of uncured patch on Al substrate

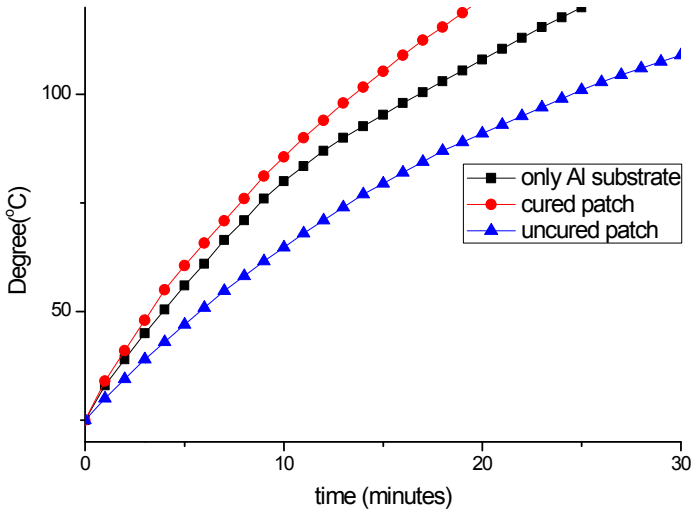

(a) Simulation

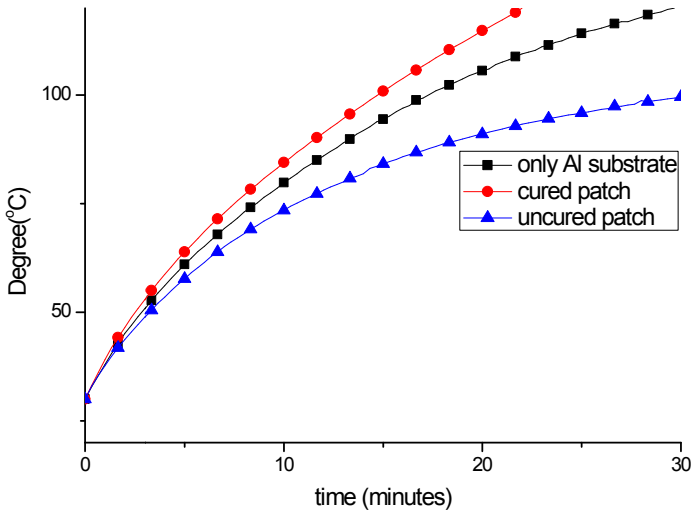

(b) Experiment

Figure 4.12 Comparison of experimental and simulation results

Table 4.1 Material property of simulation for induction heating

	Air	Al	Coil	Cured patch	Uncured prepreg
Relative permeability	1	1	1	1	1
Resistivity(Ωm)	-	27e-9	17e-9	2.7e-4	1e20
Thermal conductivity (w/m ℃)	-	165	401	0.3	0.294
Specific heat(J/kg ℃)	-	875	385	1255	1150
Density(kg/m$^{3)}$	-	2770	8300	1572	1900

Chapter 6

SUMMARY AND CONCLUSIONS

Chapter 6
Summary and conclusions

We investigated the feasibility of using induction heating as a means of curing adhesives and patches in composite bonded joints. It was found that the induction-cured DLS samples exhibited bond strengths very similar to those of the corresponding oven-cured samples; this was true for both baseline as well as CNT-reinforced samples. Therefore, induction heating can be considered an effective technique for curing adhesives and patches during composite patch bond repairs.

The bond strengths of the DLS samples were also found to depend on the fabrication method used. Cocured patch samples (fabricated by oven or induction curing) exhibited higher bond strengths than those of the corresponding precured patch samples; this was true for both baseline and CNT-reinforced samples. The cocured patch samples had a more undulated bondline profile than did the precured patch samples. It is believed that an undulated bondline profile results in greater bond strength. Therefore, the bond strengths of the cocured patch samples were higher than those of the corresponding precured patch samples.

For both the precured and the cocured samples, it was shown that the

dispersion of 0.5 wt% CNTs in the adhesive improved bond strength. The CNT-reinforced samples exhibited slightly higher bond strengths than did the baseline samples. When CNTs are inserted on both sides of the adhesive layer, the strength of the adhesive interface layer between the adhesive and the substrates is enhanced.

Finally, it was shown experimentally and numerically that the uncured patches decreased the temperature increase rate during induction heating. However, this should not be a critical issue in real-life applications. With regard to the induction heating of an aluminum substrate alone as well as the heating of an assembly consisting of a precured patch and an aluminum substrate, the experimental results and those of numerical simulations were similar. The temperature of the aluminum substrates increased more rapidly in the case of precured patches than in the case of cocured patches. Thus, it can be concluded that induction curing and the cocuring method are sound and efficient techniques for the bonding and repair of metallic aircraft structures.

REFERENCES

REFERENCES

[1] F. F. Fabrizio Ricci, Nicola Montefusco, "Bonded Composite Patch Repairs on Cracked Aluminum Plates- Theory, Modeling and Experiments," *Advances in Composites Materials,* pp. 445-463, 2011.

[2] F. R. Alan Baker, Rhys Jones, "Advances Repair Metallic Aircraft Structure vol. 1," *Book,* 2002.

[3] S. Mahdi, H.-J. Kim, B. Gama, S. Yarlagadda, and J. W. Gillespie, "A comparison of oven-cured and induction-cured adhesively bonded composite joints," *Journal of Composite Materials,* vol. 37, pp. 519-542, 2003.

[4] G. Tsamasphyros, I. Prassianakis, A. Christopoulos, G. Kanderakis, and K. Kalkanis, "Non destructive testing of bonded composite repairs using embedded metallic grids–numerical analysis," *NDT for Safety,* November 07–09, 2007.

[5] S. Yarlagadda, H. J. Kim, J. W. Gillespie, N. B. Shevchenko, and B. K. Fink, "A study on the induction heating of conductive fiber reinforced composites," *Journal of Composite Materials,* vol. 36, pp. 401-421, 2002.

[6] Y. Kwon, R. Slaff, S. Bartlett, and T. Greene, "Enhancement of composite scarf joint interface strength through carbon nanotube reinforcement," *Journal of materials science,* vol. 43, pp. 6695-6703, 2008.

[7] G. L. Burkholder, Y. W. Kwon, and R. D. Pollak, "Effect of carbon nanotube reinforcement on fracture strength of composite adhesive joints," *Journal of materials science,* vol. 46, pp. 3370-3377, 2011.

[8] Y. W. Kwon and A. Marrón, "Scarf Joints of Composite Materials: Testing and Analysis," *Applied Composite Materials,* vol. 16, pp. 365-378, 2009/12/01 2009.

[9] "C-141 Composite Material Repairs to Metallic Airframe Components," *Structural integrity program,* vol. 1993, pp. 728-756, 1993.

[10] J. Schubbe and S. Mall, "Investigation of a cracked thick aluminum panel repaired with a bonded composite patch," *Engineering Fracture Mechanics,* vol. 63, pp. 305-323, 1999.

[11] R. J. C. A.A. Baker, M.J. Davis, R. Jones, J.G. Williams, "Repair of mirage III aircraft using the BFRP crack-patching technique," *Theoretical and Applied Fracture Mechanics,* vol. 2, pp. 1-15, 1984.

[12] L. R. F. Rose, "An application of the inclusion analogy for bonded reinforcements," *International journal of solids and structures,* vol. 17, pp. 827-838, 1981.

[13] J. Klug, S. Maley, and C. T. Sun, "Characterization of fatigue behavior of bonded composite repairs," *Journal of aircraft,* vol. 36, pp. 1016-1022, 1999.

[14] S. Mall and S. Naboulsi, "Modeling of a cracked metallic structure with bonded composite patch using the three layer technique," *Composite Structures,* vol. 35, pp. 295-308, 1996.

[15] S. Naboulsi and S. Mall, "Nonlinear analysis of bonded composite patch repair of cracked aluminum panels," *Composite Structures,* vol. 41, pp. 303-313, 1998.

[16] K. H. Chung and W. H. Yang, "Fracture mechanics analysis on the bonded repair of a skin/stiffener with an inclined central crack," *Composite Structures,* vol. 55, pp. 269-276, 2002.

[17] P. Cheuk, L. Tong, C. Wang, A. Baker, and P. Chalkley, "Fatigue crack growth in adhesively bonded composite-metal double-lap joints," *Composite Structures,* vol. 57, pp. 109-115, 2002.

[18] J. Wang, A. Rider, M. Heller, and R. Kaye, "Theoretical and experimental research into optimal edge taper of bonded repair patches subject to fatigue loadings," *International journal of adhesion and*

adhesives, vol. 25, pp. 410-426, 2005.

[19] A. Mahadesh Kumar and S. Hakeem, "Optimum design of symmetric composite patch repair to centre cracked metallic sheet," *Composite Structures,* vol. 49, pp. 285-292, 2000.

[20] J. Schubbe and S. Mall, "Modeling of cracked thick metallic structure with bonded composite patch repair using three-layer technique," *Composite Structures,* vol. 45, pp. 185-193, 1999.

[21] V. K. Srivastava, "Effect of carbon nanotubes on the strength of adhesive lap joints of C/C and C/C–SiC ceramic fibre composites," *International journal of adhesion and adhesives,* vol. 31, pp. 486-489, 2011.

[22] S. Y. H. J. Kim1, B. K. Fink, and J. W. Gillespie, Jr., "Through-thickness heating behavior of carbon fiber reinforced prepreg stacks in induction heating process(2002-11-34th sampe tech-v34-pp1192-1204)," 2002.

[23] R. Mathur, S. G. Advani, S. Yarlagadda, and B. K. Fink, "Genetic Algorithm Based Resistive Susceptor Design for Uniform Heating During the Induction Bonding Process," *Journal of Thermoplastic Composite Materials,* vol. 16, pp. 529-550, 2003.

[24] Charles F. Tiffany, "Aging of U.S Airforce aircraft," 1997.

[25] F. R. Alan Baker, Rhys Jones, "Advances repair metallic aircraft structure vol.2," *Book,* 2002.

[26] A. 1-1H-39, "Aircraft battle damage repair technical order."

[27] A. Baker, "Bonded composite repair of fatigue-cracked primary aircraft structure," *Composite Structures,* vol. 47, pp. 431-443, 1999.

[28] S.-C. Her, "Stress analysis of adhesively-bonded lap joints," *Composite Structures,* vol. 47, pp. 673-678, 1999.

[29] L. Hart-Smith, *Adhesive-bonded double-lap joints*: National Aeronautics and Space Administration, 1973.

[30] V. Rudnev, *Handbook of induction heating*. New York: Marcel Dekker, 2003.

[31] L. A. Barragán, D. Navarro, J. Acero, I. Urriza, and J. M. Burdío, "FPGA implementation of a switching frequency modulation circuit for EMI reduction in resonant inverters for induction heating appliances," *Industrial Electronics, IEEE Transactions on,* vol. 55, pp. 11-20, 2008.

[32] M. Jungwirth and D. Hofinger, "Multiphysics Modelling of High-Frequency Inductive Devices," in *The Proceeding of the COMSOL Users conference*, 2007.

[33] D. Istard, "Induction heating process design using COMSOL," 2010.

[34] www.gpgyjr.com.cn, "Theory of heating by induction."

[35] M. R. Kamal and S. Sourour, "Kinetics and thermal characterization of thermoset cure," *Polymer Engineering & Science,* vol. 13, pp. 59-64, 1973.

[36] P. Musto, E. Martuscelli, G. Ragosta, P. Russo, and P. Villano, "Tetrafunctional epoxy resins: modeling the curing kinetics based on FTIR spectroscopy data," *Journal of Applied Polymer Science,* vol. 74, pp. 532-540, 1999.

[37] S. H. Ahn and G. S. Springer, "Repair of Composite Laminates-II: Models," *Journal of Composite Materials,* vol. 32, pp. 1076-1114, 1998.

[38] Dr. A.K.M. AL-Shaikhli*, "FEM-Simulation of single and multi layered induction heating systems," *Eng.& Tech. Journal,* vol. Vol.27, pp. 2245-2262, 2009.

[39] M. N. O. Sadiku, *Numerical techniques in electromagnetics*. Boca Raton, Fla.: CRC Press, 1992.

[40] W. H. Hayt, *Engineering electromagnetics 6th ed* vol. 6th ed. New York: McGraw-Hill, 2001.

[41] D. Landek, F. Cajner, and T. Filetin, "Computer simulation of induction surface hardening axially symmetric workpieces," *Journal de physique. IV, Proceedings,* vol. 120, pp. 499-506, 2004.

[42] V. S. Nemkov, R. C. Goldstein, V. A. Bukanin, A. Zenkov, and D. Koutchmassov, "Computer simulation of induction heating and quenching processes," *Quenching and control of distortion,* vol. 1999, pp. 370-377, 1999.

유도가열을 통한 항공기 구조물 복합재 패치 접착수리

서울대학교 대학원
기계항공공학부
김 민 호

요약(국문초록)

노후항공기가 늘어남에 따라서, 항공기 구조물에 예상하지 못한 많은 결함들이 발생되고 있다. 이에 많은 항공기 구조물 수리 방법이 개발되어 왔으나, 기존에 적용중인 더블러(Doubler)나 스티프너(Stiffener)를 덧대는 리벳, 볼트수리와 같은 기계적 수리 방법 외에 좀 더 효율적인 수리방법을 필요로 하고 있다. 본 논문에서는 손상을 입은 항공기 알루미늄 구조물의 복합재 패치 접착수리에 관한 내용을 연구했다. 균열이나 부식된 항공기 금속 구조물에 복합재 패치를 이용한 접착수리는 항공기 수명을 연장하고 구조물을 건전하게 유지하는 측면에서 상당히 비용적으로 효율적인 방법이다. 본 논문에서는 알루미늄 맞대기로 제작된 시편이 항공기의 손상된 구조물로 간주하

여 실험을 수행하였다. 손상된 알루미늄 시편은 유도가열방식과 오븐 가열방식으로 각각 탄소섬유 에폭시(Carbon-Epoxy)로 된 복합재 패치를 접착하여 수리하였다. 그리고 복합재 패치를 Precured 패치(패치를 미리 제작) 접착수리 방법과 Cocured(동시경화) 접착수리 방법을 사용하여 수리하였으며, 각 시편의 강도를 평가하였다. 전자기장을 이용한 유도가열방식은 접착되는 부분에 근접한 부분가열이나 신속한 가열을 할 수 있는 장점을 가지고 있다. 이러한 특성은 항공기 금속구조물의 효율적인 수리를 가능하게 한다. 유도가열방식은 패치수리 강화 시 평평하거나 굴곡된 부위를 수리할 때 사용되는 접착제나 복합소재 레진을 큐어링(curing)하는데 필요한 열원 공급방법으로 이상적인 방법이다. 유도가열 방식이 항공기 금속 구조물 수리에 효율적인 열원으로 사용될 수 있다는 것을 실험적인 방법과 수치적인 모사 방법으로 비교하였다. 본 논문의 또 다른 주제는 접착 시 접착라인에 탄소나노튜브(CNT)를 첨가함으로써 얼마나 강도 향상을 시킬 수 있는지도 연구되었다.

위의 실험결과로서, 기본시편과 탄소나노튜브(CNT)로 강화된 시편에서 각각 유도가열로 접착 수리된 시편이 오븐가열로 접착 수리된 시

편과 유사한 강도를 가짐을 알았다. 또한 기본시편과 탄소나노튜브(CNT)로 강화된 시편 모두 동시경화방식(Cocured)으로 제작된 시편이 Precured 패치 방식으로 제작된 시편보다 강도가 더 강하다는 것을 알 수 있었다. 그리고 동시경화방식(Cocured)으로 제작된 시편과 Precured 패치로 제작된 시편 각각 0.5wt%의 탄소나노튜브(CNT) 분산 용액으로 접착라인을 강화한 효과가 시편 구조물의 강도 향상을 가져온 것으로 보인다. 이러한 결과들을 볼 때, 손상된 구조물의 복합재 패치 접착수리를 통한 강도향상을 위해 유도가열 방식과 동시경화 방식, 그리고 접착라인에 탄소나노튜브(CNT) 강화 방법은 복합재 패치 접착 수리에 건전하고 효율적인 방법이 될 수 있다.

주요어 : 항공기 구조물, 복합재 패치 수리, 접착제, 유도가열,
접착 조인트, 탄소나노튜브

학 번 : 2010-30787